LA-UR-12-22510
Approved for public release; distribution is unlimited.

Title:	Non-Linear Transmission Line (NLTL) Microwave Source Lecture Notes the United States Particle Accelerator School
Author(s):	Russell, Steven J. Carlsten, Bruce E.
Intended for:	United States Particle Accelerator School, 2012-06-18/2012-06-29 (Grand Rapids, Michigan, United States)

Non-Linear Transmission Line (NLTL) Microwave Source

How NLTL Microwave Sources Work

Objective: We will quickly go through the history of the non-linear transmission lines (NLTLs). We will describe how they work, how they are modeled and how they are designed.

Note that the field of high power, NLTL microwave sources is still under development, so this is just a snap shot of their current state.

Topics:
Introduction to solitons and the KdV equation
The lumped element non-linear transmission line
Solution of the KdV equation
Non-linear transmission lines at microwave frequencies
Numerical methods for NLTL analysis
Unipolar versus bipolar input
High power NLTL pioneers
Resistive versus reactive load
Non-lineaer dielectrics
Effect of losses

John Scott Russell

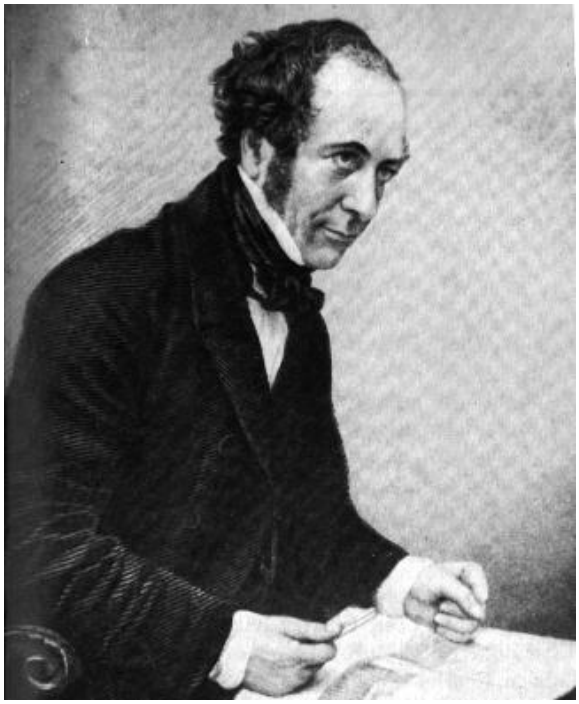

Figure 1: John Scott Russell

- **Born:** May 9, 1808 in Glasgow, Scotland
- **Died:** June 8, 1882 on the Isle of Wight

In brief, John Scott Russell graduated from Glasgow University in 1825 at the age of 17. He moved to Edinburgh University after graduation where he taught mathematics. Intellectually gifted, Russell's main contributions came as a Scottish naval engineer.

So why do we care about this guy?

The Wave of Translation

Figure 2: 1995 recreation of the original John Scott Russell Wave of Translation. (Photo from Nature v. 376, 3 August 1995, p. 373)

In 1834, while conducting experiments aimed at developing more efficient canal boat hull designs, John Scott Russell made an observation that was truly ahead of its time (by about 100 years) [1].

"*I was observing the motion of a boat which was rapidly drawn along a narrow channel by a pair of horses, when the boat suddenly stopped - not so the mass of water in the channel which it had put in motion; it accumulated round the prow of the vessel in a state of violent agitation, then suddenly leaving it behind, rolled forward with great velocity,*

assuming the form of a large solitary elevation, a rounded, smooth and well-defined heap of water, which continued its course along the channel apparently without change of form or diminution of speed. I followed it on horseback, and overtook it still rolling on at a rate of some eight or nine miles an hour, preserving its original figure some thirty feet long and a foot to a foot and a half in height. Its height gradually diminished, and after a chase of one or two miles I lost it in the windings of the channel. Such, in the month of August 1834, was my first chance interview with that singular and beautiful phenomenon which I have called the **Wave of Translation**."

Solitons

What John Scott Russell called a Wave of Translation we now know as solitons, or sometimes solitary wave when there is only one. He was quite convinced that what he had seen was very important and immediately built a 30 foot wave tank at his home and began making observations of these waves.

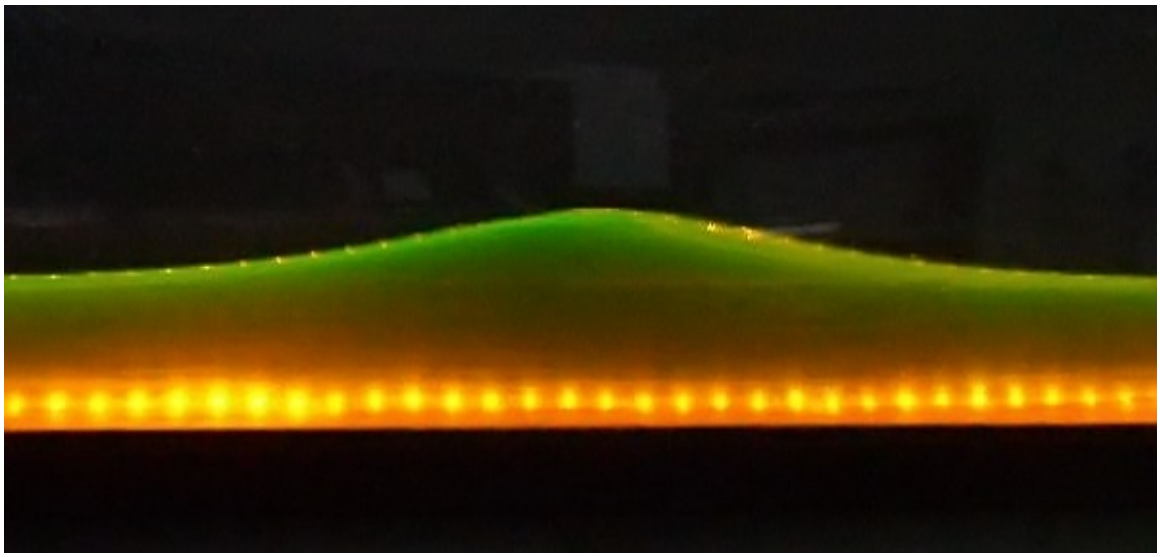

Figure 3: Solitary wave in a laboratory wave channel. (ShareAlike 2.5)

Russell's key observations were:

1. Solitons are stable and can travel over very large distances without losing their shape. (The don't disperse or break.)
2. Their speed depends on their amplitude, or height.
3. Their width depends on the depth of the water.
4. Solitons do not merge and when they collide they do not add together as traditional waves do. Colliding solitons will pass through each other without affecting each other's shape.

5. A wave that is too big for the depth of the water will split into two, one big and small.

The problem with Scott Russell's observations were that they clashed with what was then known about hydrodynamics. In particular theories developed by Isaac Newton and Daniel Bernoulli, which were essentially linear.

Solitons Continued...

Here we see two solitons colliding. Note how they pass through each other without either changing its final shape. They also don't interfere constructively as we are used to observing. This is the kind of behavior that befuddled scientists at the time.

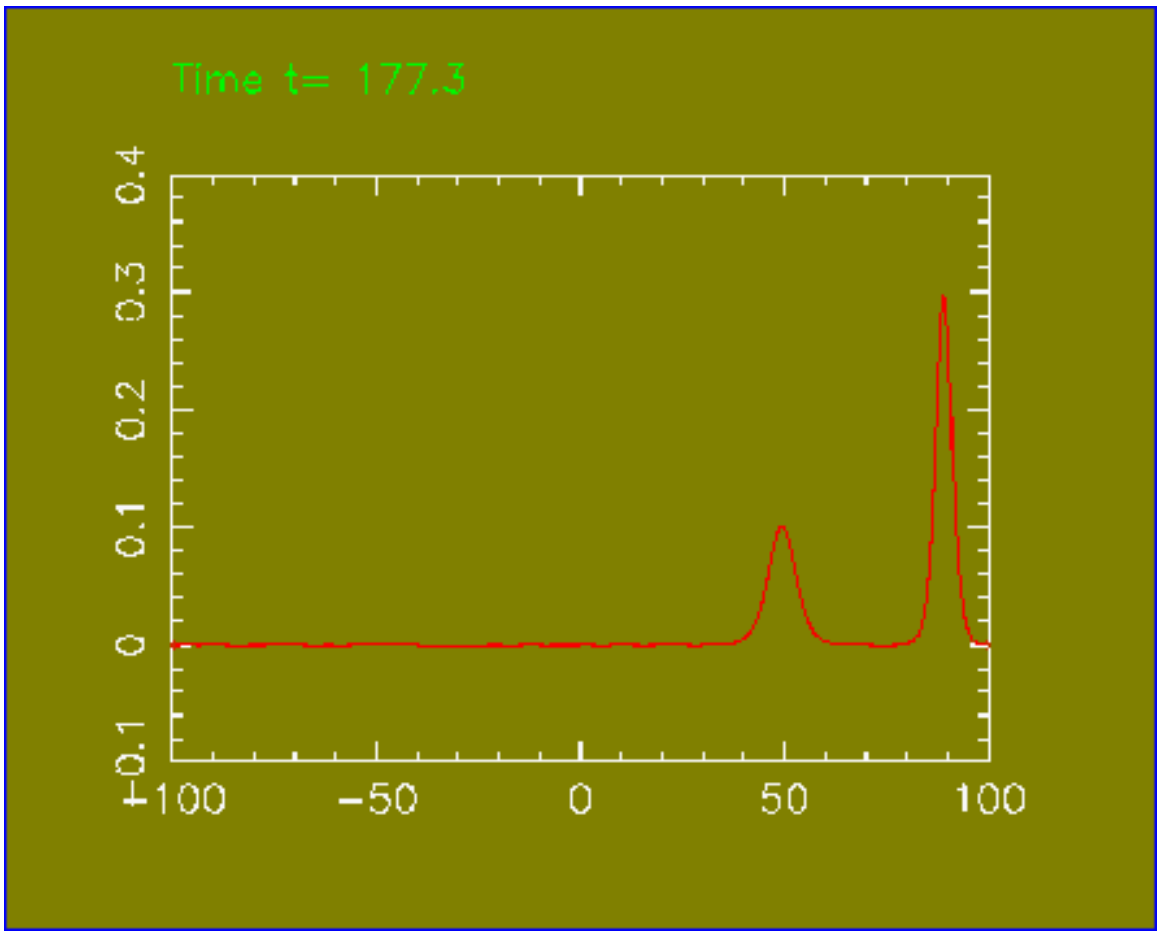

Figure 4: Video of Colliding Solitons.

Solitons Continued...

Figure 5: Video of soliton in wave tank. ("soliton splash 27 sept run 3.mp4", Author: woutzweers, Standard YouTube License)

Soliton Theory

In 1871 a fellow by the name of Joseph Valentin Boussineq published a paper that supported John Scott Russell's observations theoretically. This was quickly followed by an 1876 paper on the subject in Philosophical Magazine by Lord Rayleigh. However, the definitive treatment of the subject didn't come until 1895 in a paper by D.J. Korteweg and G. de Vries [2]:

D.J. Korteweg and G. de Vries, "On the Change of Form of Long Waves Advancing in a Rectangular Canal and on a New Type of Long Stationary Wave", *Philosophical Magazine*, 5th series **39**, p. 422-443 (1895).

This paper gave us the famous Korteweg de Vries equation:

$$\frac{du}{dt} + \alpha u \frac{du}{dx} + \beta \frac{d^3u}{dx^3} = 0 \tag{1}$$

The KdV equation has several different forms and has many solutions, both single soliton solutions and multiple soliton solutions. We will get back to it later and derive a single soliton solution. For now, though, we will just state that solitons arise due to two competing effects:

1. **Dispersion:** Dispersion works to spread the wave.
2. **Non-linear velocity:** The velocity of the wave has a non-linear dependence with height. Taller parts of the wave travel faster. This tends to focus the wave and, if left to its own devices, will cause the wave to break (Figure 6). This is what we see as waves break onto shore.

When these two effects are in balance, they create a stable wave, or soliton.

Figure 6: Breaking wave. (Steve Jurvetson, Creative Commons Attribution 2.0 Generic)

Solitons are Found Everywhere

As it turned out, John Scott Russell's discovery, which he thought was very important, essentially stayed a curiosity for about 100 years. But in 1953 it was "re-discovered" when Enrico Fermi, John R. Pasta, Stanislaw Ulam and Mary Tsingou put together a numerical simulation (FPU experiment) at Los Alamos of a vibrating string that included a non-linear term. Fermi thought that, after an initial exitation, the system would undergo thermalization so that all the energy would leak out of the original mode, exciting all of the other modes. However, the simulation showed a much more complicated quasi-periodic behavior which they could not explain.

In 1965 Norman Zabusky and Martin Kruskal demonstrated soliton behavior in media subject to the Korteweg de Vries equation in a computer simulation using the finite difference approach. At the same time, they showed that this also explained the FPU experiment.

As scientist began to understand solitons, we started to see them everywhere. (Or at least it is speculated that soliton like effects are the cause of strange behavior we see around us. Often it is very hard to prove as the math gets very complicated.)

Figure 7: Roll cloud solitons. This picture is from Queensland, Australia between Burketown and Normanton where the phenomena is frequent and called a Morning Glory cloud. (Mick Petroff, Creative Commons Attribution-Share Alike 3.0 Unported)

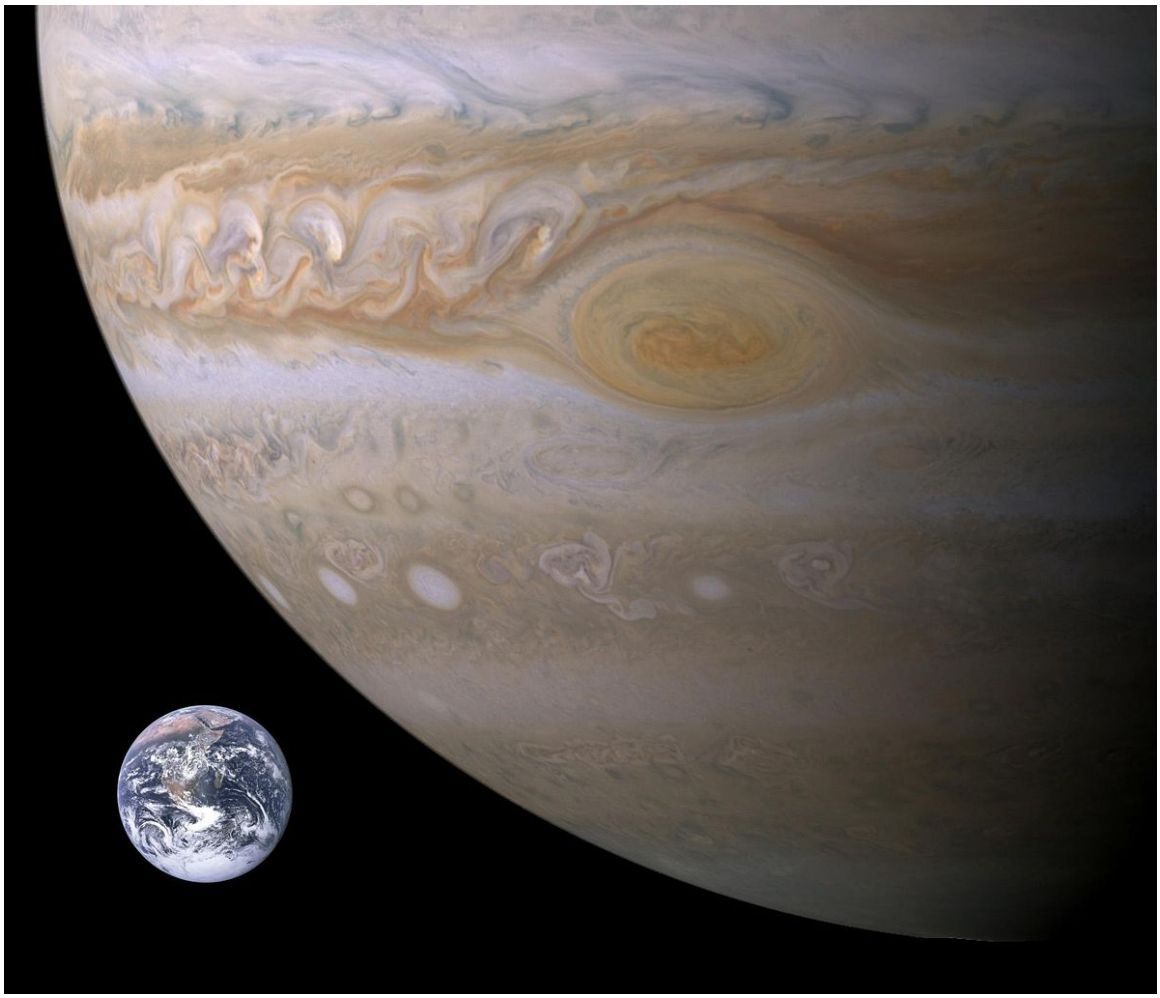

Figure 8: It is speculated that the Red Spot of Jupiter is a soliton phenomena. Here it is shown with a scale Earth for size comparison. (PD-USGOV-NASA)

Falaco Soliton

A very cool 3D soliton phenomena is the Falaco Soliton.

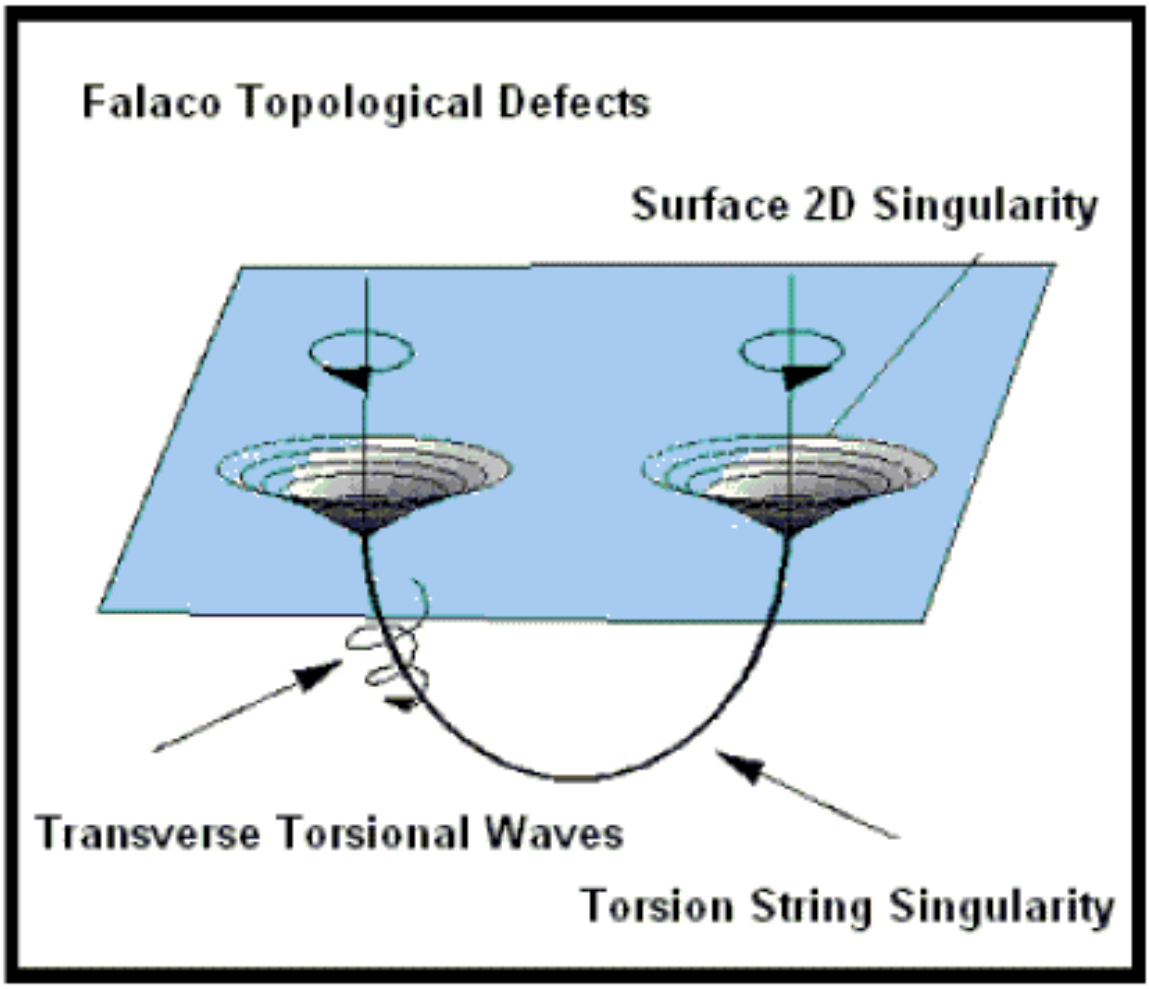

Figure 9: Diagram of Falaco Solitons. If the tube that ties them together is cut, they will immediately disappear. [3]

Figure 10: Video of Falaco Soliton. (Falaco Soliton, Author: 1O6C9LWOU, Standard YouTube License)

Optical Solitons

A very important application of solitons is in digital, fiber optic communication. A well defiined wave that does not spread as it travels down a fiber is ideal for sending 1's and 0's.

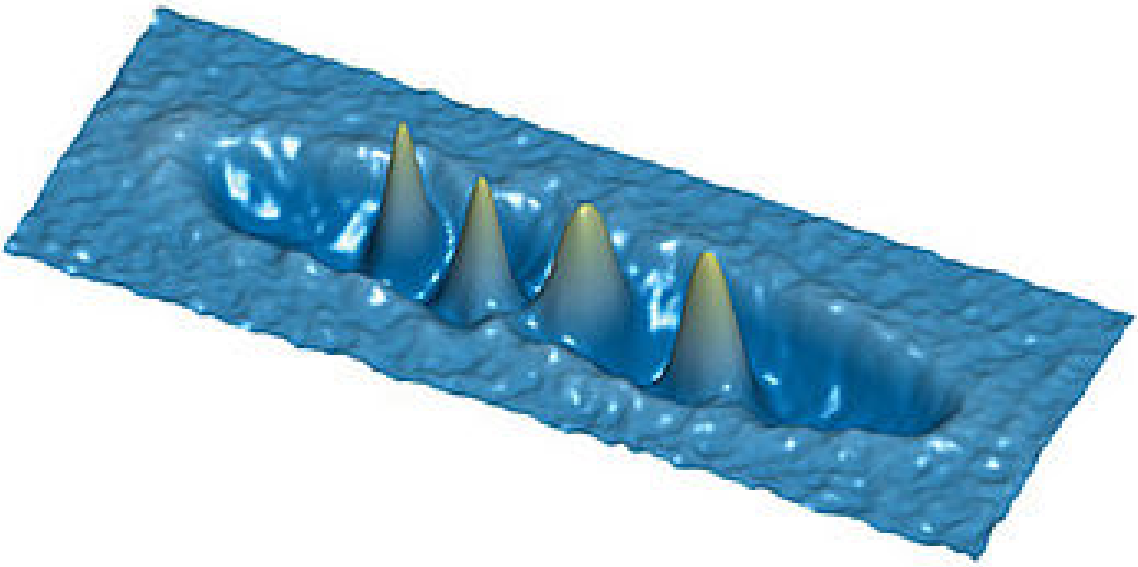

Figure 11: Optical solitons. [4]

Tidal Bores

We now come to the question of what all of this means. How does it apply to generating microwaves? To explain that, we will first turn to a very interesting phenomena called a tidal bore. (At first glance this may seem unrelated, but in fact its an exact physical analogy to NLTLs.)

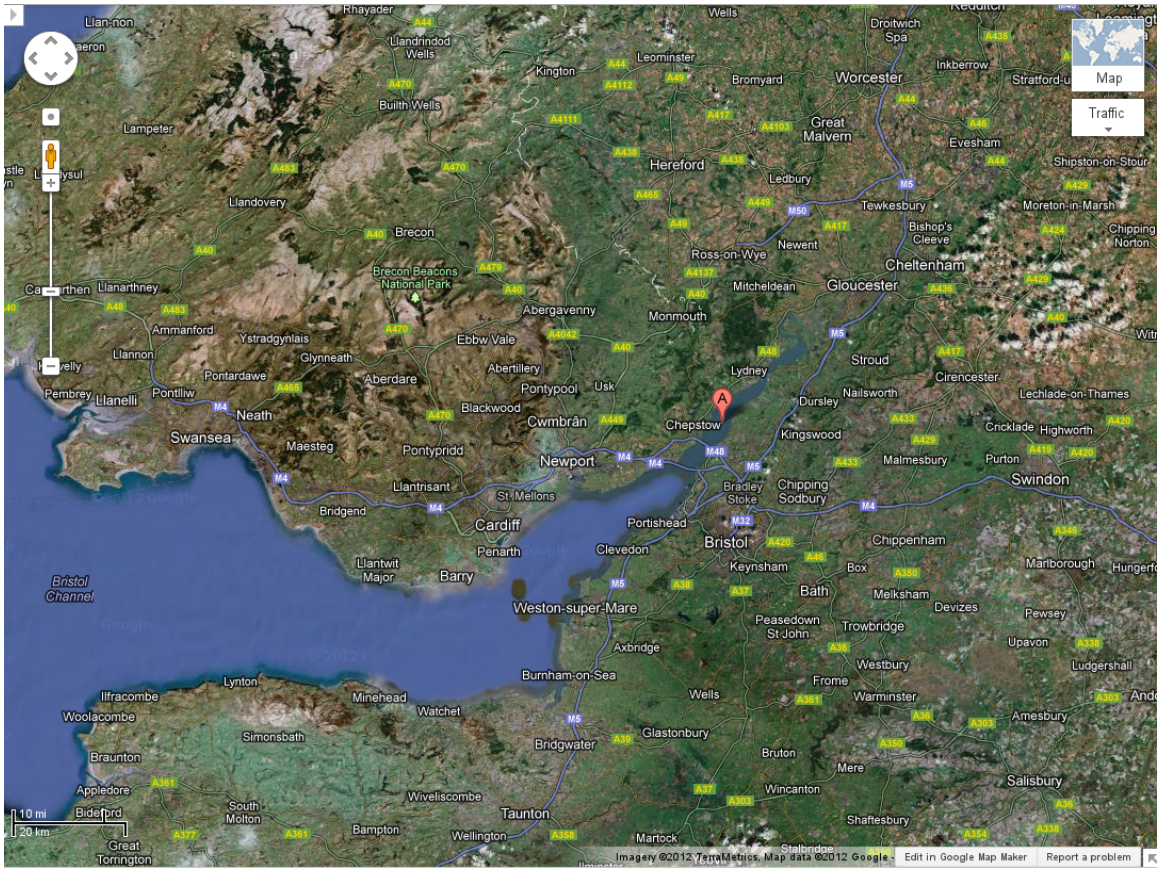

Figure 12: River Severn, United Kingdom. (Google Maps)

The River Severn is the longest river in Great Britain and has one of the highest tidal ranges in the world (48 feet). It is one of about 100 rivers on the planet that experiences something called a tidal bore. The shape of the river's estuary is essentially that of a funnel. The two banks slowly converge to the river's mouth, while at the same time the bottom of the estuary slopes up. In electrical terms, this provides good coupling between the tidal surge and the river itself. The result is a large, powerful wave being launched into the river in the upstream direction at high tide. (This is analogous to a pulsed power system providing a large voltage pulse to a conventional microwave system.)

Once this large wave is injected into the river system, the non-linear physics (aka KdV equation) kicks in. The result is the original wave breaks into a series of solitons moving up the river. These waves are much smaller in length and closely spaced. In other words, we have up-converted a low frequency, high power wave into a much higher frequency signal.

Figure 13: Video of the Severn Bore. (Chasing the Severn Bore by Paramotor 2/3/2010, Author: pjenni12, Standard YouTube License)

Figure 14: River Severn, United Kingdom to Maisemore. (Google Maps)

One of the great past times is surfing the Severn Bore, which can take a surfer quite some distance. A weir (kind of like a dam) on the river at Maisemore tends to limit this activity to the stretch of river down stream.

Figure 15: Surfing on the Severn Bore.

Can We Create the Severn Bore Electrically? Derivation of the KdV Equation for Electrical Transmission Lines

The answer is yes. This is what we call an NLTL.

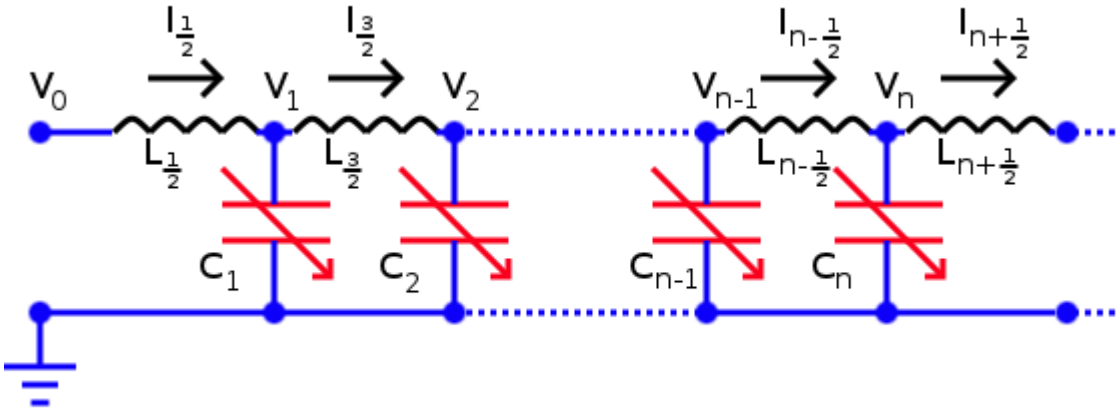

Figure 16: Transmission line lumped element circuit diagram.

For the next few pages we will follow the analysis found in the Ph.D. thesis of Martin Brown [5]

Consider a simple transmission line as depicted in Figure 16. The charge on capacitor, C_n is given by

$$Q_n = C_n(V_n)V_n$$

where we have assumed that the capacitance has some dependence on

the voltage. The current through the capacitor is then given by

$$I_n = \frac{dQ_n}{dt} = \frac{d}{dt}\left[C_n(V_n)V_n\right]$$

In turn, by conservation of charge, this current is equal to the difference between the currents flowing through the inductors to either side.

$$\frac{d}{dt}\left[C_n(V_n)V_n\right] = I_{n-\frac{1}{2}} - I_{n+\frac{1}{2}} \tag{2}$$

The voltage drop across the inductor, $L_{n-\frac{1}{2}}$, is

$$V_n - V_{n-1} = -\frac{d}{dt}LI_{n-\frac{1}{2}} = -L\frac{d}{dt}I_{n-\frac{1}{2}} \tag{3}$$

where we assume that all of the inductors are constant and equal. Taking the time derivative of Equation 2 and using Equation 3 we get

$$L\frac{d^2}{dt^2}\left[C_n(V_n)V_n\right] = V_{n-1} - 2V_n + V_{n+1} \tag{4}$$

Let's now assume that the spacing between lumped elements is δx and that the voltage is continuous function of x, $V(x,t)$:

$$\begin{aligned} V_n(t) &= V(n\delta x, t) \\ V_{n+1}(t) &= V\left[(n+1)\delta x, t\right] \\ V_{n-1}(t) &= V\left[(n-1)\delta x, t\right] \end{aligned}$$

Doing a 4^{th} order Taylor's expansion gives us

$$\begin{aligned} V_{n+1} = V\left[(n+1)\delta x, t\right] \approx & V(n\delta x, t) + \delta x \frac{\partial V}{\partial x} \\ & + \frac{\delta x^2}{2}\frac{\partial^2 V}{\partial x^2} + \frac{\delta x^3}{6}\frac{\partial^3 V}{\partial x^3} \\ & + \frac{\delta x^4}{24}\frac{\partial^4 V}{\partial x^4} + \dots \end{aligned}$$

and

$$\begin{aligned} V_{n-1} = V\left[(n-1)\delta x, t\right] \approx & V(n\delta x, t) - \delta x \frac{\partial V}{\partial x} \\ & + \frac{\delta x^2}{2}\frac{\partial^2 V}{\partial x^2} - \frac{\delta x^3}{6}\frac{\partial^3 V}{\partial x^3} \\ & + \frac{\delta x^4}{24}\frac{\partial^4 V}{\partial x^4} - \dots \end{aligned}$$

Defining the inductance per unit length, L', and the capacitance per unit length, C', we have $L = L'\delta x$ and $C = C'\delta x$. Using this and our Taylor's expansions, Equation 4 becomes

$$L'\frac{\partial^2 \left[C'(V)V(x,t)\right]}{\partial t^2} \approx \delta x^2 \frac{\partial^2 V(x,t)}{\partial x^2} + \frac{\delta x^2}{12}\frac{\partial^4 V(x,t)}{\partial x^4} \tag{5}$$

Introducing a general function for the non-linearity of the capacitance per unit length

$$C'(V)V = C'_0\left(V + f(V)\right)$$

where $f(V)$ is a function that describes the non-linearity and C_0' is a constant, Equation 5 becomes

$$\frac{\partial^2 V(x,t)}{\partial t^2} + \frac{\partial^2 f(V)}{\partial t^2} \approx \frac{1}{L'C_0'}\left(\frac{\partial^2 V(x,t)}{\partial x^2} + \frac{\delta x^2}{12}\frac{\partial^4 V(x,t)}{\partial x^4}\right) \tag{6}$$

We now continue to follow Brown, but he in turn followed Washimi and Taniuti [6]. Express $V(x,t)$ as a power series expansion in the small parameter $\epsilon < 1$:

$$V(x,t) = \epsilon V^{(1)}(x,t) + \epsilon^2 V^{(2)}(x,t) + \ldots$$

where $V^{(1)}$ is a first order approximation, $V^{(2)}$ is a second order approximation etc. Using Equation 6 we get for the first order term:

$$\frac{\partial^2 V^{(1)}}{\partial t^2} + \frac{1}{\epsilon}\frac{\partial^2 f(V)}{\partial t^2} \approx \frac{1}{L'C_0'}\left(\frac{\partial^2 V^{(1)}(x,t)}{\partial x^2} + \frac{\delta x^2}{12}\frac{\partial^4 V^{(1)}(x,t)}{\partial x^4}\right) \tag{7}$$

Changing the coordinates to a system moving at velocity $c = \frac{1}{\sqrt{L'C_0'}}$, we have:

$$\xi = \epsilon^{\frac{1}{2}}(x - ct)$$
$$\tau = \epsilon^{\frac{3}{2}}ct$$
$$\frac{\partial}{\partial x} = \frac{\partial}{\partial \xi}\left(\frac{\partial \xi}{\partial x}\right) + \frac{\partial}{\partial \tau}\left(\frac{\partial \tau}{\partial x}\right) = \epsilon^{\frac{1}{2}}\frac{\partial}{\partial \xi}$$
$$\frac{\partial^2}{\partial x^2} = \epsilon\frac{\partial^2}{\partial \xi^2}$$
$$\frac{\partial^4}{\partial x^4} = \epsilon^2\frac{\partial^4}{\partial \xi^4}$$
$$\frac{\partial}{\partial t} = \frac{\partial}{\partial \xi}\left(\frac{\partial \xi}{\partial t}\right) + \frac{\partial}{\partial \tau}\left(\frac{\partial \tau}{\partial t}\right) = -c\epsilon^{\frac{1}{2}}\frac{\partial}{\partial \xi} + \epsilon^{\frac{3}{2}}c\frac{\partial}{\partial \tau}$$
$$\frac{\partial^2}{\partial t^2} = \epsilon c^2\left(\epsilon\frac{\partial}{\partial \tau} - \frac{\partial}{\partial \xi}\right)\left(\epsilon\frac{\partial}{\partial \tau} - \frac{\partial}{\partial \xi}\right) = \epsilon c^2\left(\epsilon^2\frac{\partial^2}{\partial \tau^2} - 2\epsilon\frac{\partial^2}{\partial \xi \partial \tau} + \frac{\partial^2}{\partial \xi^2}\right)$$

Substituting all this mess into Equation 7 gives us

$$\epsilon c^2\left(\epsilon^2\frac{\partial^2 V^{(1)}}{\partial \tau^2} - 2\epsilon\frac{\partial^2 V^{(1)}}{\partial \xi \partial \tau} + \frac{\partial^2 V^{(1)}}{\partial \xi^2}\right) + c^2\left(\epsilon^2\frac{\partial^2 f}{\partial \tau^2} - 2\epsilon\frac{\partial^2 f}{\partial \xi \partial \tau} + \frac{\partial^2 f}{\partial \xi^2}\right)$$
$$\approx c^2\left(\epsilon\frac{\partial^2 V^{(1)}}{\partial \xi^2} + \epsilon^2\frac{\delta x^2}{12}\frac{\partial^4 V^{(1)}}{\partial \xi^4}\right)$$

Keeping terms to order ϵ^2 we get:

$$2\frac{\partial^2 V^{(1)}(\xi, \tau)}{\partial \xi \partial \tau} - \frac{\partial^2 f(V)}{\partial \xi^2} + \frac{\delta x^2}{12}\frac{\partial^4 V^{(1)}(\xi, \tau)}{\partial \xi^4} = 0 \tag{8}$$

At this point, we make yet another approximation for the non-linearity of the capacitance:

$$
\begin{aligned}
f(V) &= -\alpha \left(V^{(1)} \right)^2 \\
\frac{\partial f}{\partial \xi} &= -2\alpha V^{(1)} \frac{\partial V^{(1)}}{\partial \xi} \\
\frac{\partial^2 f}{\partial \xi^2} &= -2\alpha \left(\frac{\partial V^{(1)}}{\partial \xi} \right)^2 - 2\alpha V^{(1)} \frac{\partial^2 V^{(1)}}{\partial \xi^2}
\end{aligned}
$$

Substituting the second derivative of f into Equation 8 we get:

$$
\frac{\partial^2 V^{(1)}}{\partial \xi \partial \tau} + \alpha \left(\frac{\partial V^{(1)}}{\partial \xi} \right)^2 + \alpha V^{(1)} \frac{\partial^2 V^{(1)}}{\partial \xi^2} + \frac{\delta x^2}{24} \frac{\partial^4 V^{(1)}}{\partial \xi^4} = 0
$$

Integrating this equation with respect to ξ leaves:

$$
\frac{V^{(1}}{\partial \tau} + \alpha V^{(1)} \frac{\partial V^{(1)}}{\partial \xi} + \frac{\delta x^2}{24} \frac{\partial^3 V^{(1)}}{\partial \xi^3} = 0 \tag{9}
$$

This, you may recognize, as equivalent to the KdV equation, Equation 1.

Solution of the KdV Equation

To solve Equation 9 we will first rewrite it in a simplified form.

$$\frac{\partial \phi}{\partial t} + \alpha\phi\frac{\partial \phi}{\partial x} + \beta\frac{\partial^3 \phi}{\partial x^3} = 0 \tag{10}$$

Again we will follow Brown, who in turn based his method on [7].

We will look for a traveling wave solution of the form

$$\phi(x,t) = f(\zeta)$$

where $\zeta = x - ct$ and c is a constant. So, we have

$$\begin{aligned}
\frac{\partial}{\partial x} &= \frac{\partial}{\partial \zeta}\left(\frac{\partial \zeta}{\partial x}\right) + \frac{\partial}{\partial t}\left(\frac{\partial t}{\partial x}\right) \\
&= \frac{\partial}{\partial \zeta} = \frac{d}{d\zeta} \\
\frac{\partial^3}{\partial x} &= \frac{d^3}{d\zeta^3} \\
\frac{\partial}{\partial t} &= \frac{\partial}{\partial \zeta}\left(\frac{\partial \zeta}{\partial t}\right) + \frac{\partial}{\partial x}\left(\frac{\partial x}{\partial t}\right) \\
&= -c\frac{\partial}{\partial \zeta} = -c\frac{d}{d\zeta}
\end{aligned}$$

In addition, we will assume that $f(\zeta)$ and all of its derivatives go to zero as $\zeta \to \infty$.

Substituting this solution into Equation 10 we get

$$-c\frac{df}{d\zeta} + \alpha f\frac{df}{d\zeta} + \beta\frac{d^3f}{d\zeta^3} = 0$$

Integrating once with respect to ζ gives us:

$$-cf + \frac{1}{2}\alpha f^2 + \beta\frac{d^2f}{d\zeta^2} = A \tag{11}$$

where A is an arbitrary constant. Taking the limit as $\zeta \to \infty$ and invoking our boundary conditions requires that $A = 0$.

Integrating Equation 11 with respect to $\frac{df}{d\zeta}$ gives us

$$\frac{1}{2}\beta\left(\frac{df}{d\zeta}\right)^2 = -\frac{1}{6}\alpha f^3 + \frac{1}{2}cf^2 + B$$

where B is an arbitrary constant. Once again taking the limit of $\zeta \to \infty$ and invoking our boundary conditions requires that $B = 0$. This leaves us with

$$\frac{\beta}{2}\left(\frac{df}{d\zeta}\right)^2 = f^2\left(\frac{1}{2}c - \frac{1}{6}\alpha f\right)$$

This can be rearranged to give:

$$\sqrt{\frac{\beta}{c}}\int \frac{\mathrm{d}f}{f\left(1 - \frac{\alpha}{3c}f\right)^{\frac{1}{2}}} = \pm\int \mathrm{d}\zeta \tag{12}$$

If we make the subsitution:

$$f = \frac{3c}{\alpha}\operatorname{sech}^2(\theta) \tag{13}$$

Equation 12 becomes:

$$\sqrt{\frac{\beta}{c}}\frac{\alpha}{3c}\int \frac{\mathrm{d}f}{\operatorname{sech}^2(\theta)\left(1-\operatorname{sech}^2(\theta)\right)^{\frac{1}{2}}} = \pm\int \mathrm{d}\zeta$$

Using the identity

$$\tanh^2(\theta) = 1 - \operatorname{sech}^2(\theta) \tag{14}$$

and we get

$$\sqrt{\frac{\beta}{c}}\frac{\alpha}{3c}\int \frac{\mathrm{d}f}{\operatorname{sech}^2(\theta)\tanh(\theta)} = \pm\int \mathrm{d}\zeta \tag{15}$$

Rearranging Equation 13 using Equation 14 gives us

$$f = \frac{3c}{\alpha}\left(1-\tanh^2(\theta)\right)$$

Differentiating

$$\begin{aligned}
\mathrm{d}f &= -\frac{3c}{\alpha}\frac{d}{d\theta}\tanh^2(\theta)d\theta \\
&= -\frac{6c}{\alpha}\tanh(\theta)\left(1-\tanh^2(\theta)\right) \\
&= -\frac{6c}{\alpha}\tanh(\theta)\,\mathrm{sech}^2(\theta)
\end{aligned}$$

Substituting $\mathrm{d}f$ into Equation 15:

$$\begin{aligned}
-2\sqrt{\frac{\beta}{c}}\int\frac{\mathrm{sech}^2(\theta)\tanh(\theta)}{\mathrm{sech}^2(\theta)\tanh(\theta)}\mathrm{d}\theta &= \pm\int\mathrm{d}\zeta \\
-2\sqrt{\frac{\beta}{c}}\int\mathrm{d}\theta &= \pm\int\mathrm{d}\zeta
\end{aligned}$$

Solving for θ gives us:

$$\theta = \mp\frac{1}{2}\sqrt{\frac{\beta}{c}}\left(\zeta + x_0\right)$$

where x_0 is an arbitrary constant. So:

$$f(\zeta) = \frac{3c}{\alpha}\,\mathrm{sech}^2\left[\mp 2\sqrt{\frac{\beta}{c}}\left(\zeta + x_0\right)\right]$$

or

$$\phi(x - ct) = \frac{3c}{\alpha} \operatorname{sech}^2 \left[\mp 2\sqrt{\frac{\beta}{c}} (x - ct + x_0) \right] \tag{16}$$

where the $\mp$ just refers to waves propagating in opposite directions.

The solution to the KdV equation shown in Equation 16 shows that the amplitude of solitons do indeed depend on their velocity, c.

For normal humans, mathematical analysis of NLTLs ends here more-or-less. When we design and analyze these lines numerical methods prove to be far more useful.

Lumped Element NLTL Circuit Example

The non-linear lumped element transmission line was discovered in the 1960s and it offered a really exciting opportunity to compare experimental measurements to both numerical and analytical theory in a one dimensional system. As a result, there are lots of publications on solitons in non-linear circuits in the decades following. As an example, we show results from Nagashima and Amagishi [8] in Figures 17, 18 and 19. This experiment, and others like it, demonstrated excellent agreement between theory and experiment.

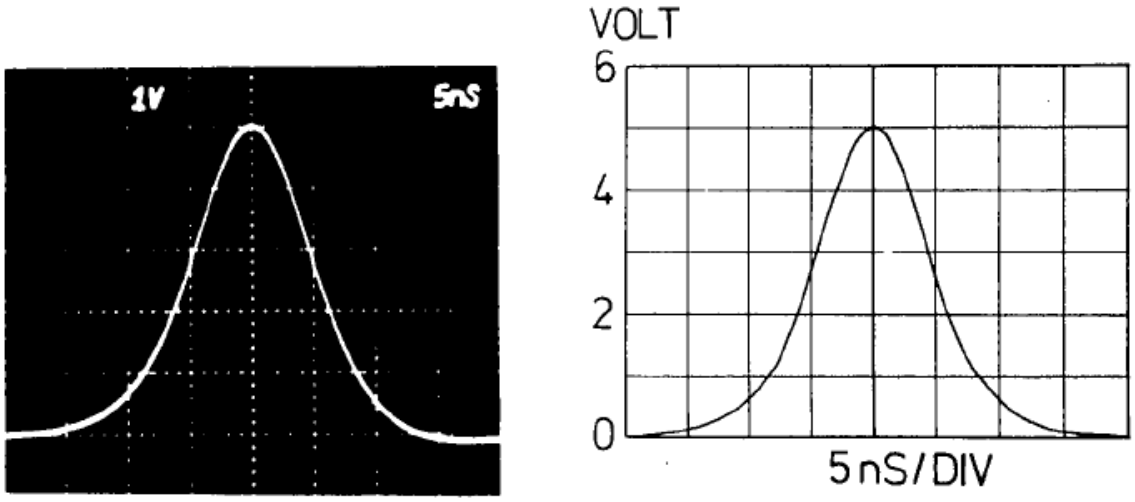

Figure 17: Comparison of the theoretical and experimental result for one soliton on a lumped element non-linear transmission line [8]. Referencing Figure 16 this photo was taken at $n = 20$. The scale is $1\frac{volt}{division}$ vertically and $5.0\frac{ns}{division}$ horizontally.

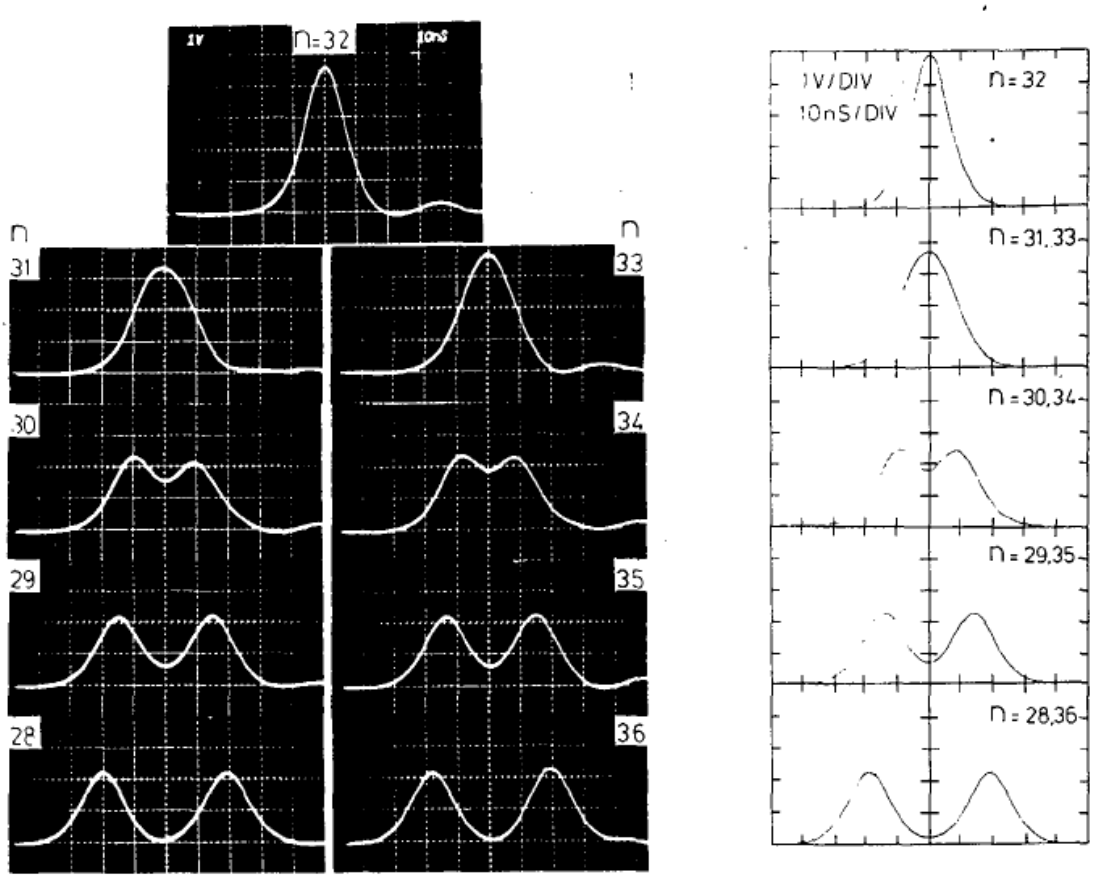

Figure 18: Comparison of the theoretical and experimental result of a head-on collision of two solitons in a lumped element non-linear transmission line [8]. The scale is $1\frac{volt}{division}$ vertically and $10.0\frac{ns}{division}$ horizontally.

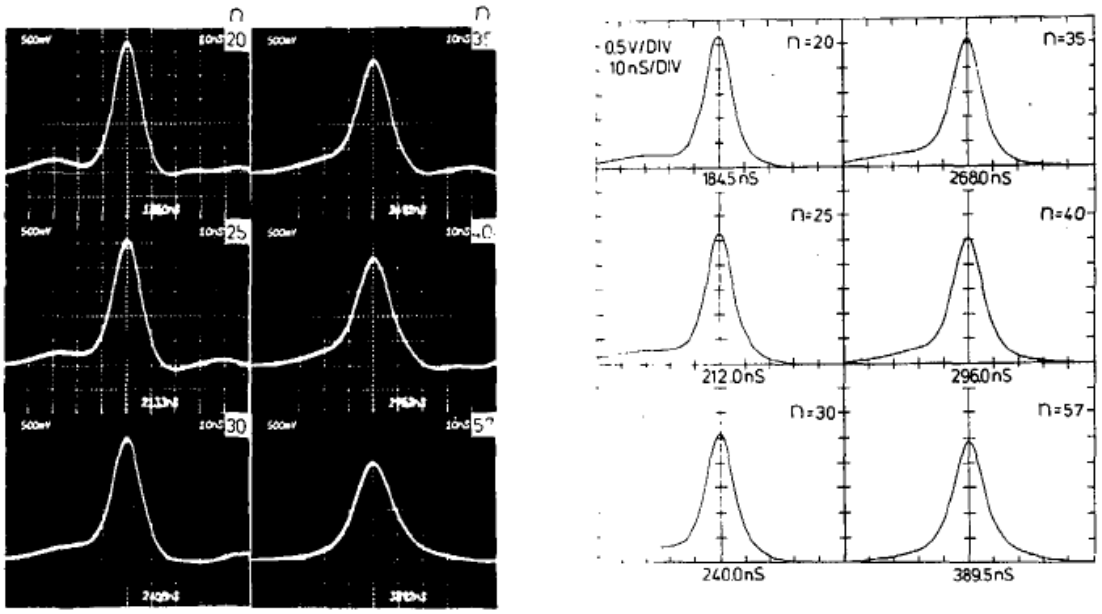

Figure 19: Comparison of the theoretical and experimental result of an overtaking collision of two solitons in a lumped element non-linear transmission line [8]. The scale is $1\frac{volt}{division}$ vertically and $10.0\frac{ns}{division}$ horizontally.

Frequency Up-Conversion with an NLTL

Propagation of solitons on NLTLs if fine, but this is not what really interests us. We want to make microwaves. It turns out, NLTLs can do this too.

In Figure 20 we show what happens schematically when a unipolar voltage input pulse is introduced into an NLTL. The pulse first develops a shock on the leading edge of the pulse due to the greater velocity of the parts of the wave with greater amplitude. When the shock is steep enough the wave breaks into solitons closely spaced in time. This forms our microwave signal.

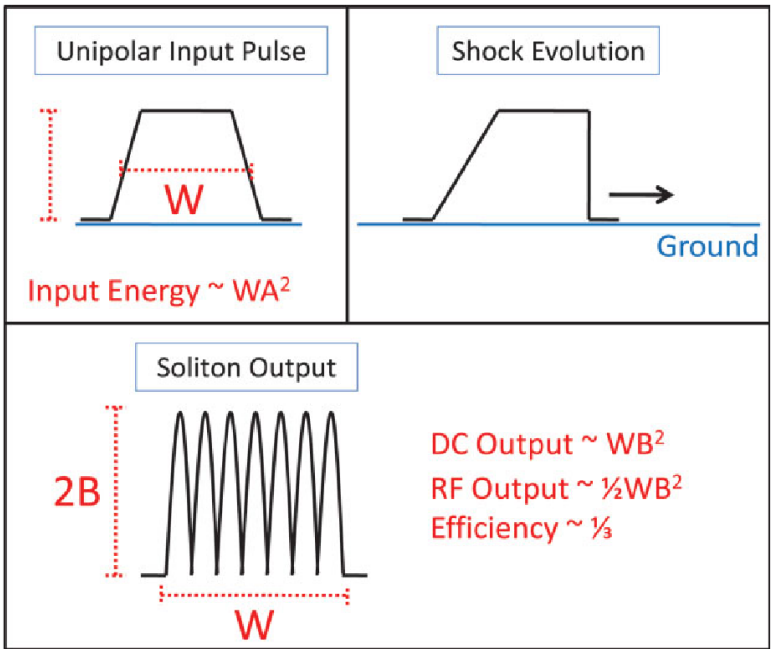

Figure 20: Schematic description of soliton formation in an NLTL when a unipolar input voltage pulse is introduce to the line [9].

In Figure 21 we show a simulation of a NLTL where we input a unipolar voltage pulse into an NLTL. An initial square input pulse develops into a series of closely spaced solitons. These solitons form a microwave signal.

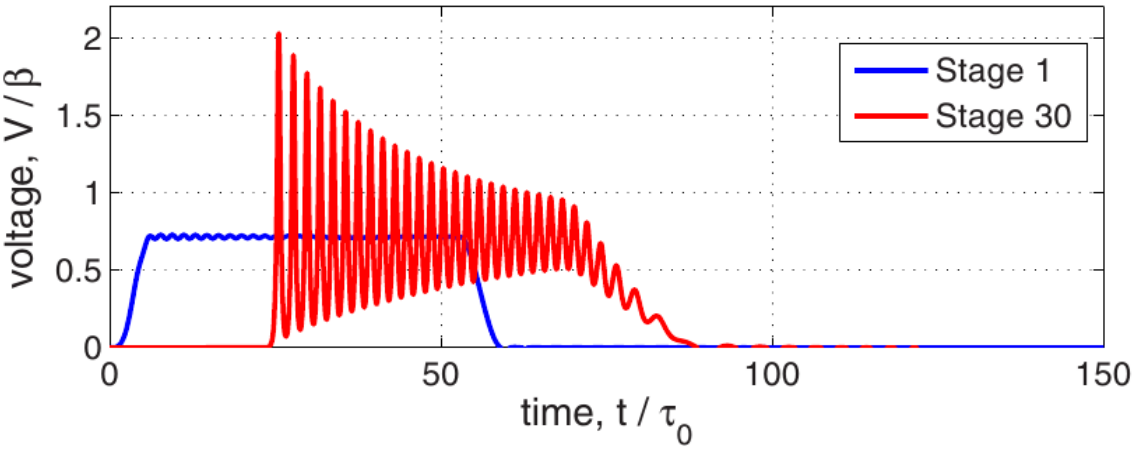

Figure 21: Numerical solution of an NLTL with an initial unipolar input voltage pulse [9].

High-Frequency NLTL

Up to now, our picture of an NLTL is a lumped element transmission line. That is, discrete capacitors, inductors etc. However, with a lumped element line we are limited to very low microwave frequencies (around 1 MHz). If we try to go above this the losses become too high. So, if we want higher microwave frequencies (100s of MHz), we use a different physical form for our NLTL. This is shown in Figure 22.

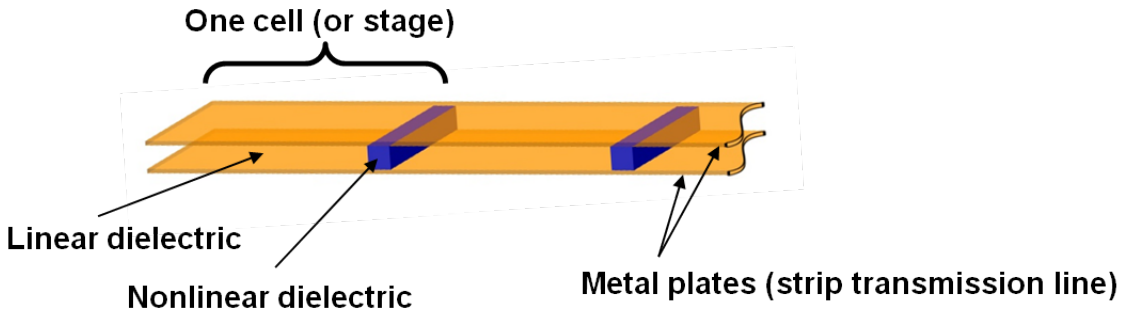

Figure 22: Parallel plate NLTL for generating high frequency microwaves. A typical NLTL will consist of 100s of cells (stages).

Figure 22 shows a parallel plate NLTL geometry. We periodically load a simple parallel plate transmission line with blocks of non-linear dielectrics. We will talk about the dielectric material in more detail later, but for now we show a typical plot of the differential dielectric constant dependence on applied electric field and temperature in Figure 23. (We will talk about the differential dielectric constant later, but the dielectric constant we are used to is basically the integral of this curve.)

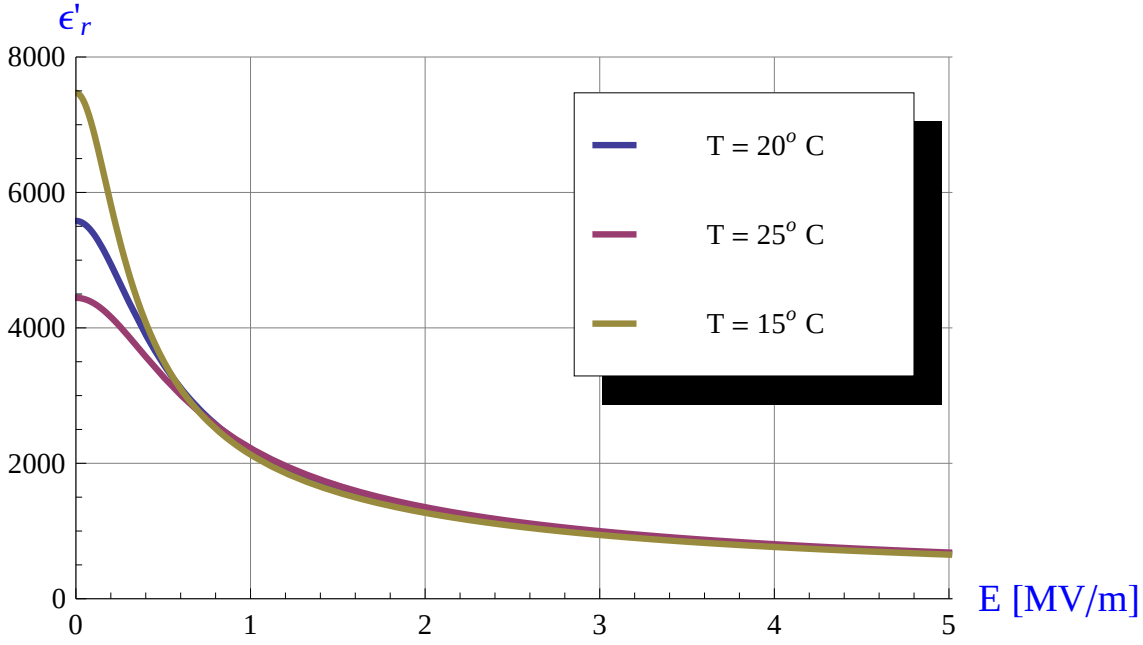

Figure 23: Differential dielectric constant versus applied electric field for BSTO. We show three different curves demonstrating the temperature dependence of the material. This is a typical property.

Although the structure in Figure 22 looks quite different physically from a lumped element line, we can generally represent it as a lumped element line to great accuracy. Consider Figure 24. The inductance and capacitance of our lumped element line in Figure 16 are given by

$$L = \frac{\mu h L_1}{w}$$
$$C(V) = \frac{\epsilon(V) w L_2}{h}$$

So, the analysis we have done for the lumped element circuit applies to the parallel plate NLTL, especially when $w \gg h$. (It also works remarkably well when this condition isn't true.)

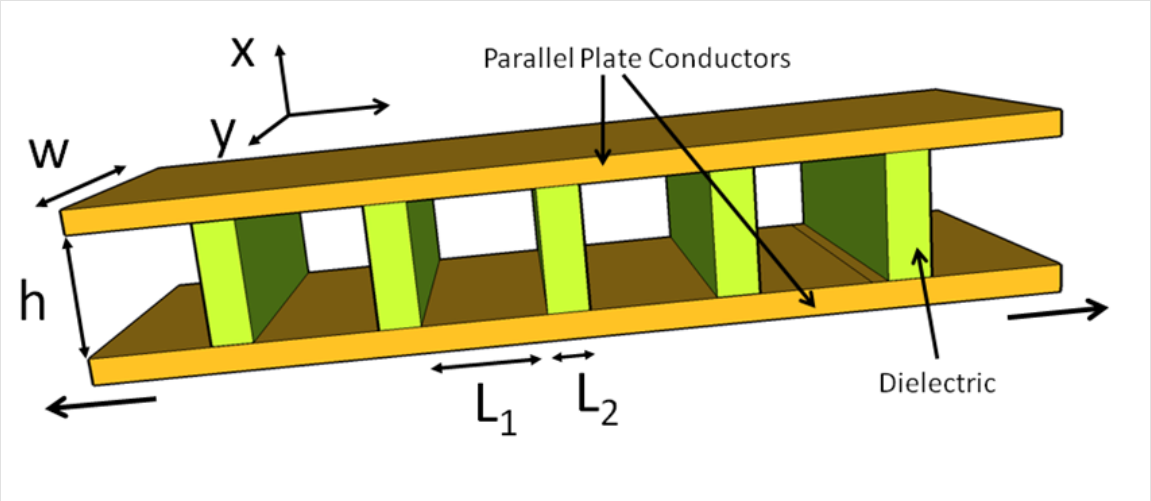

Figure 24: Parallel plate NLTL schematic.

A final note on NLTLs. The output frequency of these devices scales with the small signal frequency, defined as [9]

$$f_0 = \frac{1}{\sqrt{LC_0}} \tag{17}$$

where L is given above and C_0 is given by

$$C_0 = C\left(V = V_{bias}\right) = \frac{\epsilon\left(V = V_{bias}\right)\omega L_2}{h} \tag{18}$$

The bias voltage, V_{bias}, is the DC voltage across the metal plates of the NLTL and has been assumed to be zero up till now. How the output frequency scales with f_0 is a function of the non-linearity of the dielectric materials [9]. One of the intriguing features of NLTLs is that we can, in principle, change the frequency of an NLTL by adjusting V_{bias}

Note on Non-Linear Magnetic NLTLs

We so far have talked about non-linear dielectric loaded NLTLs. We could just as well use a non-linear magnetic material to make a non-linear magnetic line. The analysis is basically the same. However, there are a couple of practical difference between the two technologies:

1. We have mature choices for non-linear magnetic materials and so this technology is more accesible. In fact, there is a commercial magnetic NLTL that you can buy now.

2. Magnetic materials are more lossy than dielectrics, so the efficiency tends to be about 20%. In principle a dielectric line is limited to 66% efficiency.

We do not have any real experience with magnetic lines, so we won't say anything more about them. Just be aware they exist.

Numerical Methods

There are basically two ways to simulate NLTLs: numerical circuit model and the finite difference time domain (FDTD) method. We will not go into great detail here, but briefly:

1. **Circuit Model:** Here we simply integrate the circuit equations, like those we derived for Figure 16, numerically (e.g. Runge Kutta).
   - Very fast.
   - Can only do one dimension problems. It is an approximation for all other cases.
   - Losses are represented by adding resistors, which doesn't always capture the true physical picture.
2. **FDTD:** In a FDTD code an NLTL is represented by a grid in one, two or three dimensions. Maxwell's Equations are then solved numerically as a function of time on the grid.
   - Physically accurate.
   - Multidimensional.
   - Slow. Parallel codes help.
   - Representing non-linear dielectrics is hard.
   - Representing non-linear dielectrics with losses is even harder.

In general we find that the two methods give very comparable results. In Figure 25 we show a comparison of an NLTL simulated by both a 2D FDTD code and a 1D circuit code. They give very similar results. In Figure 26 we show a 3D FDTD simulation of an NLTL using the commercial code XFdtd from Remcom. In Figure 27 we show a comparison between the 3D results and a 1D circuit model of the same line. Again we see excellent agreement.

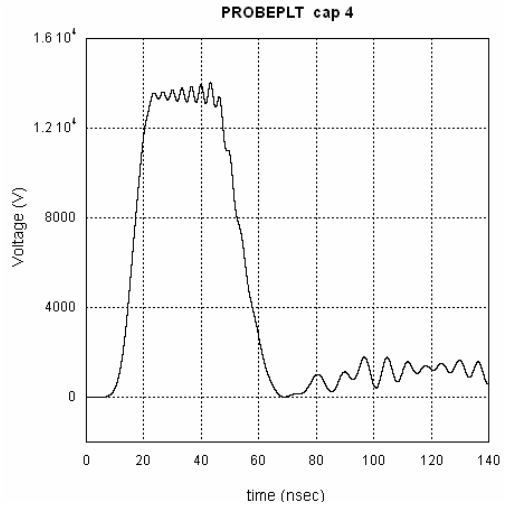

(a) 2D FDTD code result at cell #4.

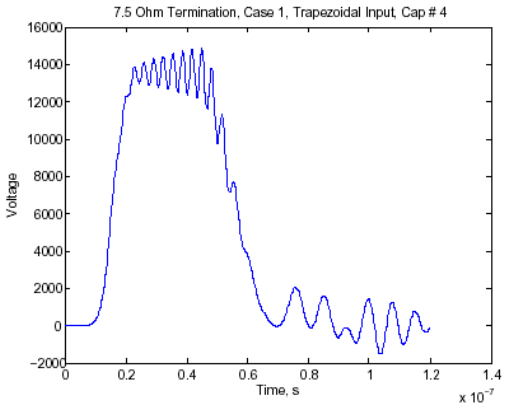

(b) 1D circuit code result at cell #4.

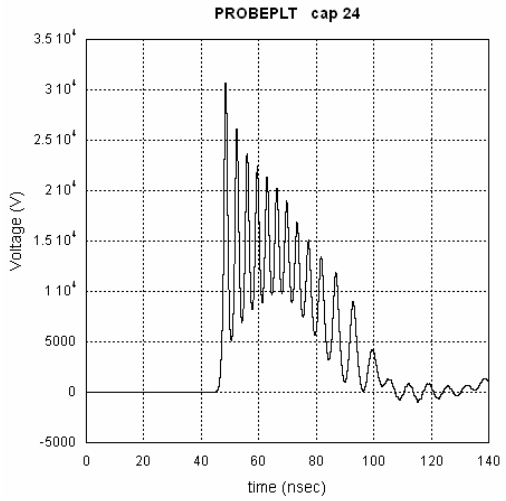

(c) 2D FDTD code result at cell #24.

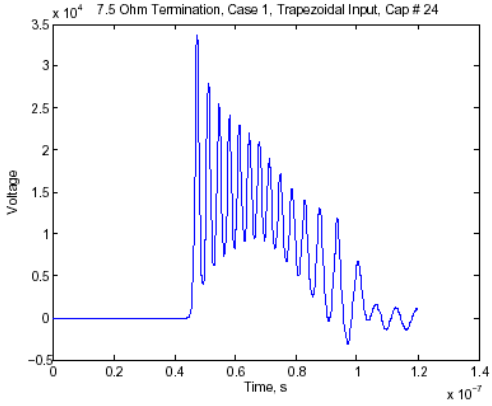

(d) 1D circuit code result at cell #24.

Figure 25: Results comparing a 2D FDTD calculation and a 1D circuit model of an equivalent NLTL.

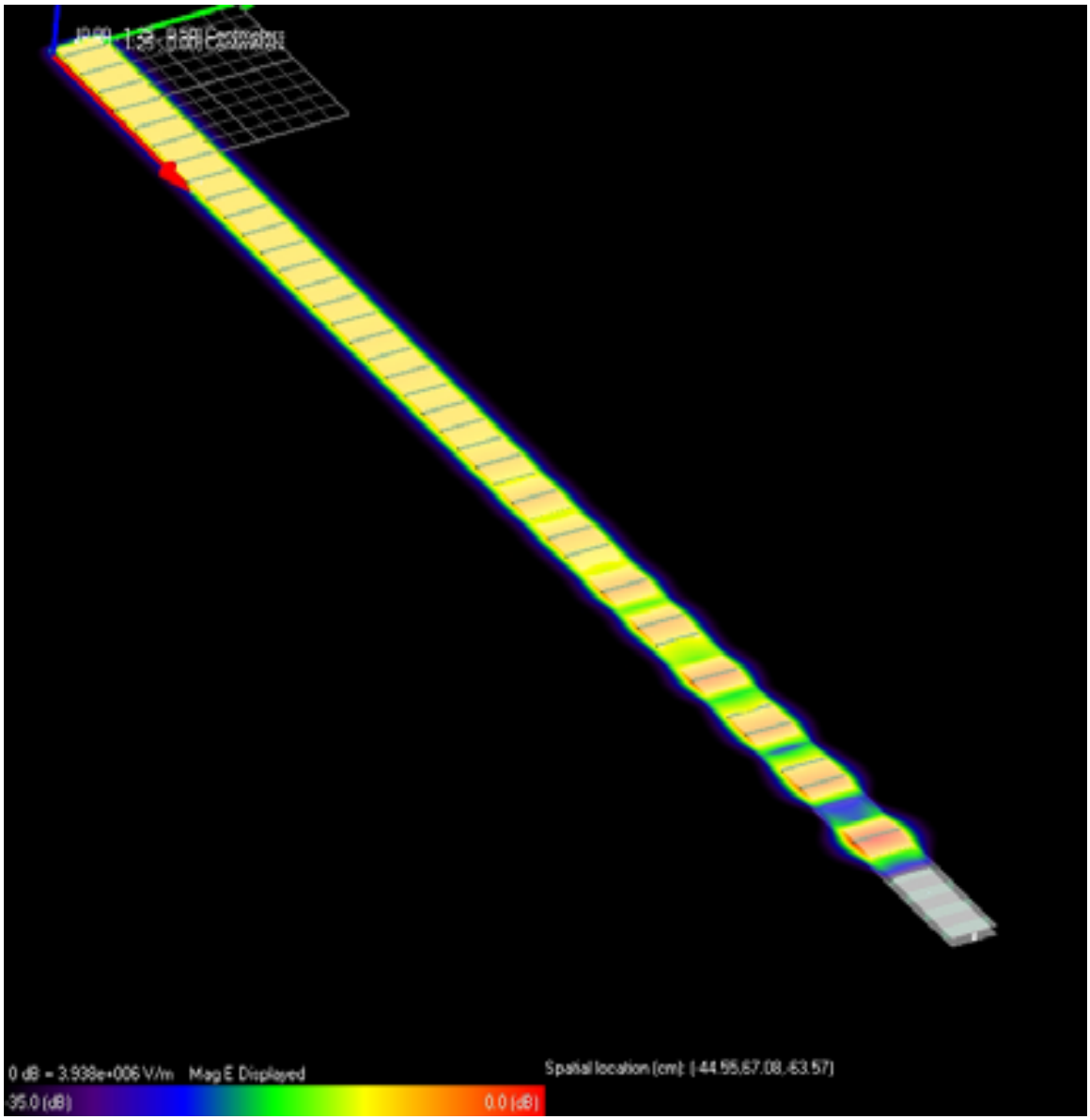

Figure 26: XFTdtd (Remcom) 3D simulation of an NLTL.

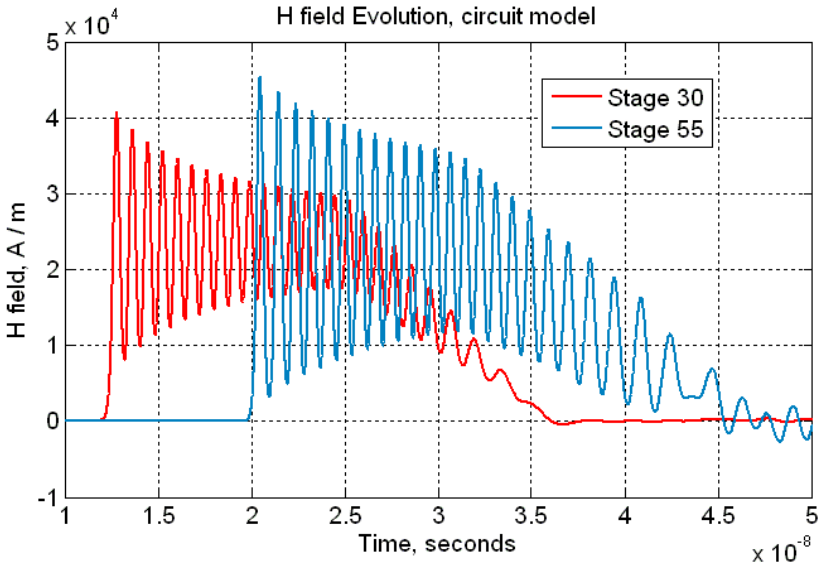

(a) 1D circuit model simulation.

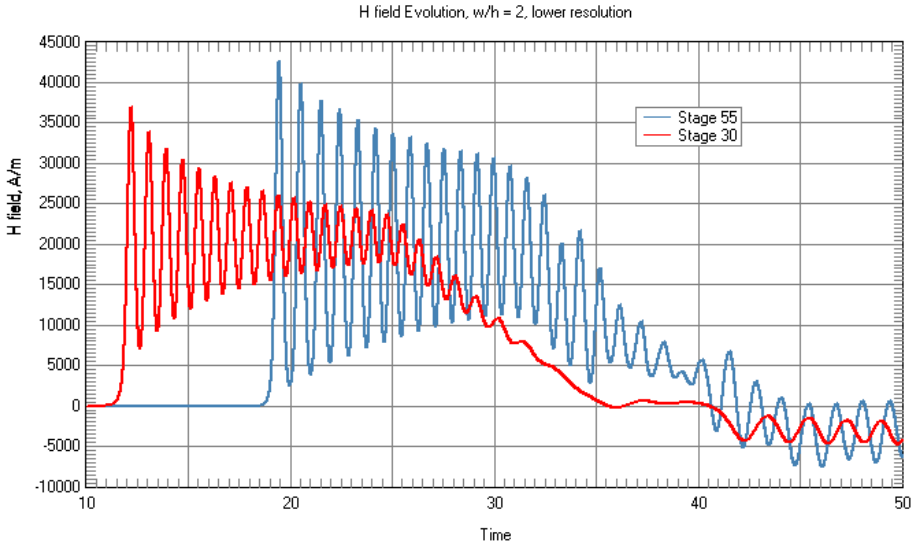

(b) 3D XFdtd simulation.

Figure 27: Results comparing a 1D circuit model simulation of the NLTL in Figure 26 to a 3D FDTD calculation of the same line using the Remcom code XFdtd.

NLTL Efficiency: Uni-polar versus Bi-polar Input Pulse

Consider Figure 28. Up till now we have assumed a uni-polar input pulse to our NLTLs. In such a situation, if the electrical losses in the line are low and the line is long enough that the solitons are allowed to fully develop (that is they go all the way to zero), then the output signal is approximately given by:

$$V(t) = B + B\sin(\omega t)$$

inside the time envelope with width $\Delta t = W$. The total energy is given by

$$E = B^2 W + \frac{1}{2} B^2 W = \frac{3}{2} B^2 W$$

so the RF efficiency is given by the energy in the RF part of the signal divided by the total energy:

$$\text{Efficiency}_{RF} = \frac{\frac{1}{2} B^2 W}{\frac{3}{2} B^2 W} = \frac{1}{3}$$

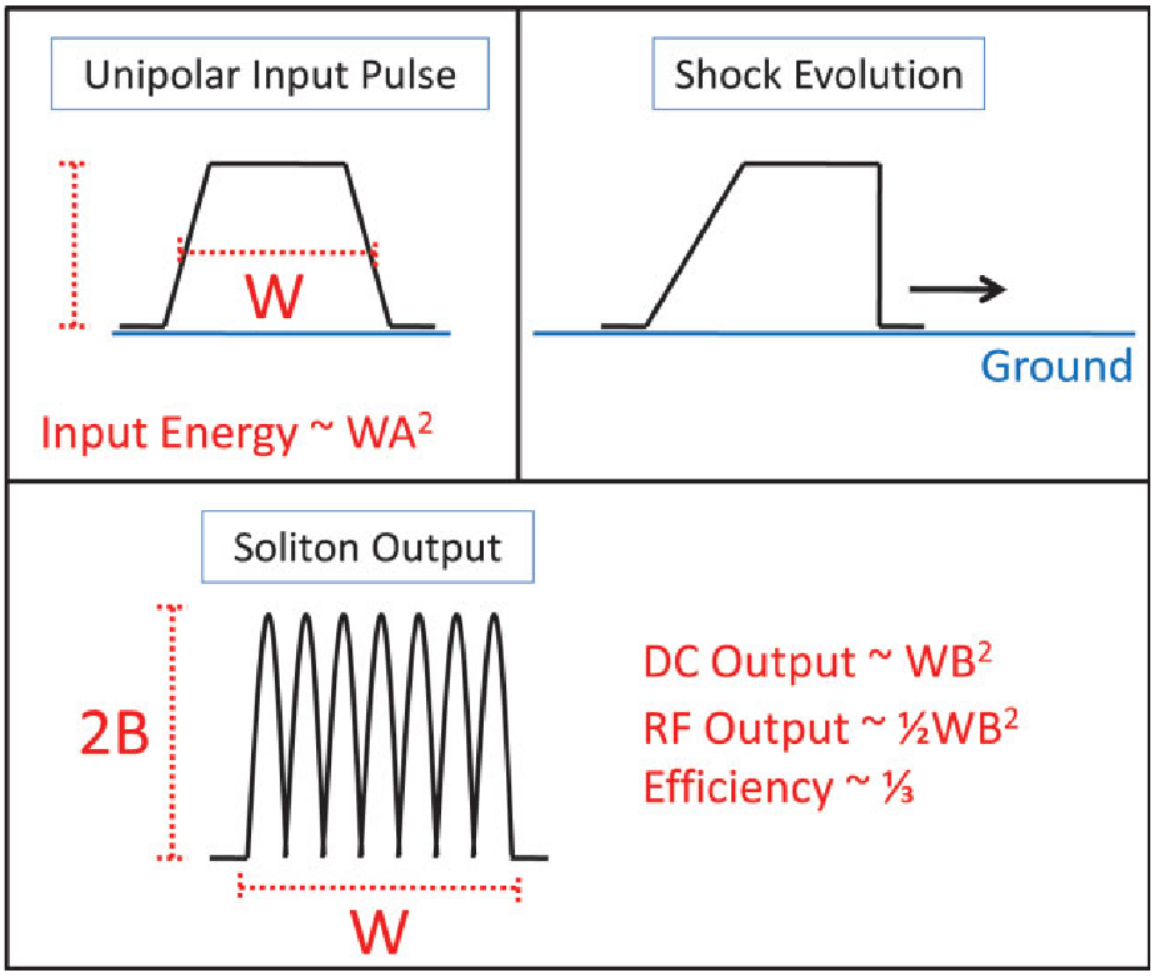

Figure 28: Schematic illustrating the efficiency of an NLTL driven by a uni-polar input pulse [10].

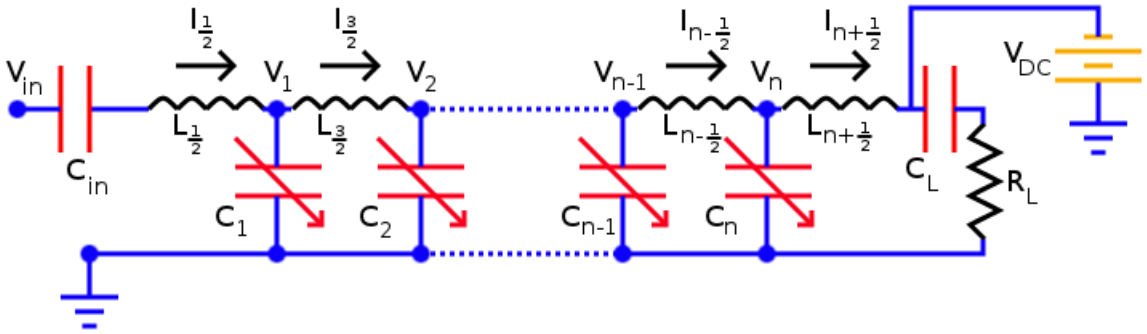

Figure 29: Biased NLTL which allows us to input a bi-polar input pulse [10].

Now, let us modify our original NLTL circuit so that it looks like that shown in Figure 29. In this case we can use a bi-polar input pulse, as illustrated in Figure 30. A bi-polar input is just two uni-polar voltage pulses following each other, with the leading pulse having a negative amplitude. If these two pulses have a width in time of $\Delta t = W$, which is the width of the uni-polar input pulse in Figure 28, and one half the amplitude, $\frac{A}{2}$, then the total input energy is

$$E_{in} = \frac{1}{2}A^2W$$

which is one half the input energy for the uni-polar input. However, if we set the DC bias voltage to $V_{DC} = \frac{A}{2}$, we can propagate the bi-polar pulse on the line shown in Figure 29. The result is a train of solitons of width $\Delta t = W$ and amplitude B, the same as for the uni-polar case. However, because the input energy is now half, the efficiency doubles to [10]

$$\text{Efficiency}_{RF} = \frac{2}{3}$$

In Figure 31 we show solitons forming on a biased NLTL showing soliton formation using a bi-polar input pulse.

Finally, one additional feature of the biased line shown in Figure 29, is that it gives us a natural way to exploit Equations 17 and 18 to adjust the output frequency of an NLTL [10].

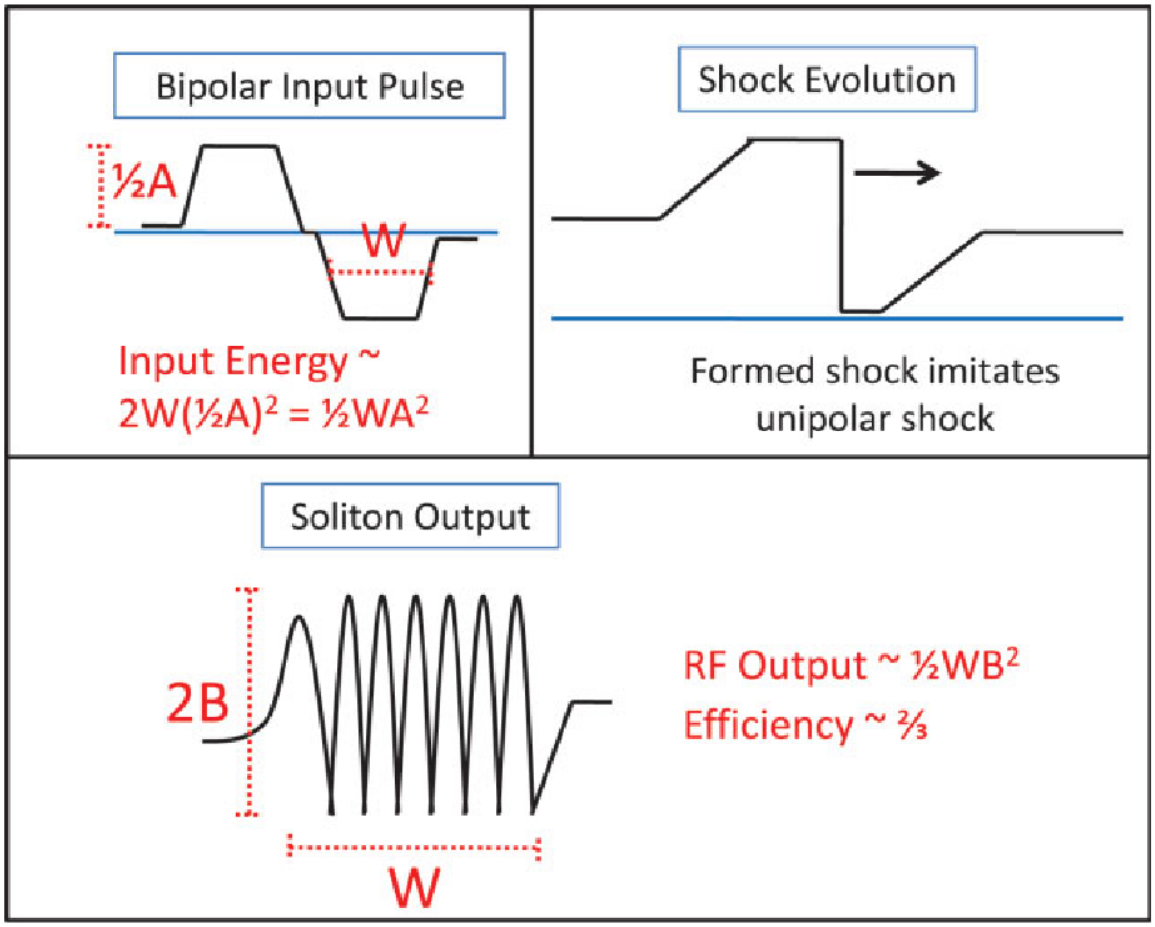

Figure 30: Schematic illustrating the efficiency of an NLTL driven by a bi-polar input pulse [10].

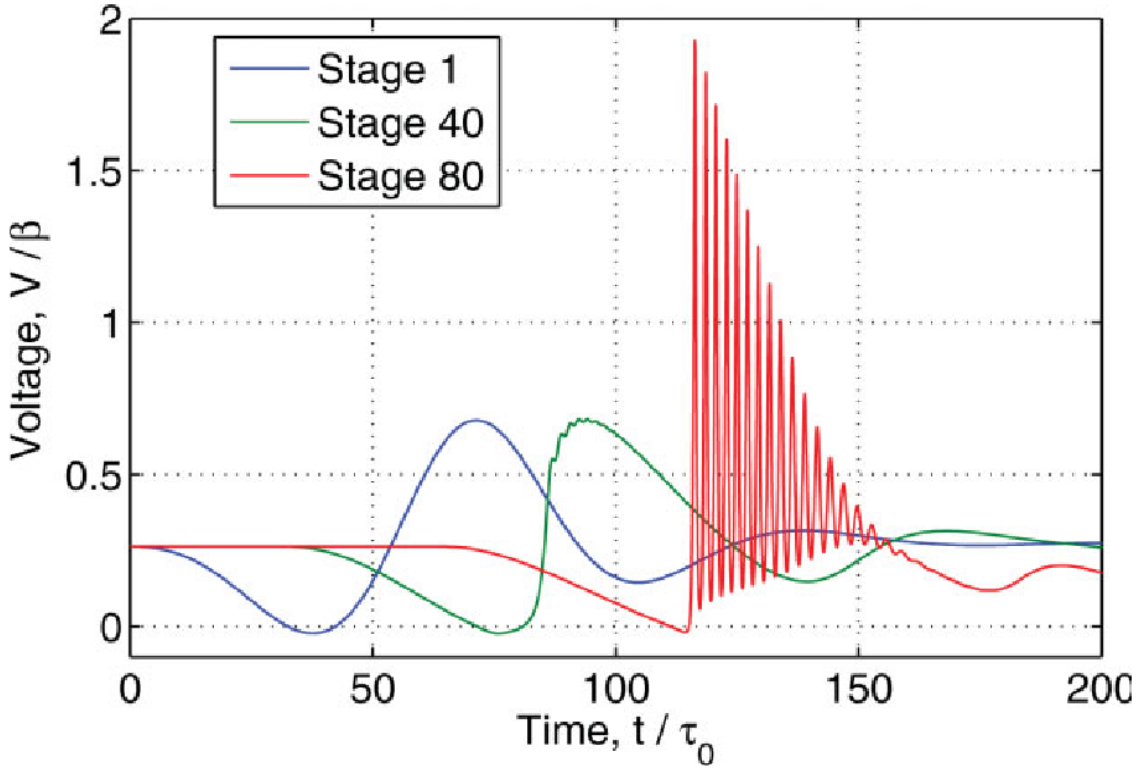

Figure 31: Simulation of a DC bias NLTL with a bi-polar input pulse [10].

High Power NLTL Pioneers

The pioneers of high frequency, high power NLTLs are Hiroyuki Ikezi of General Atomics [11] and Paul Smith [12], along with his students such as Martin Brown [5], of Oxford University. Both produced substantial peak powers from NLTLs at microwave frequencies. We show the results of one of Ikezi's high power experiments [11] in Figures 32 and 33. This line produced 7.8 MW of RF power between 200 and 400 MHz.

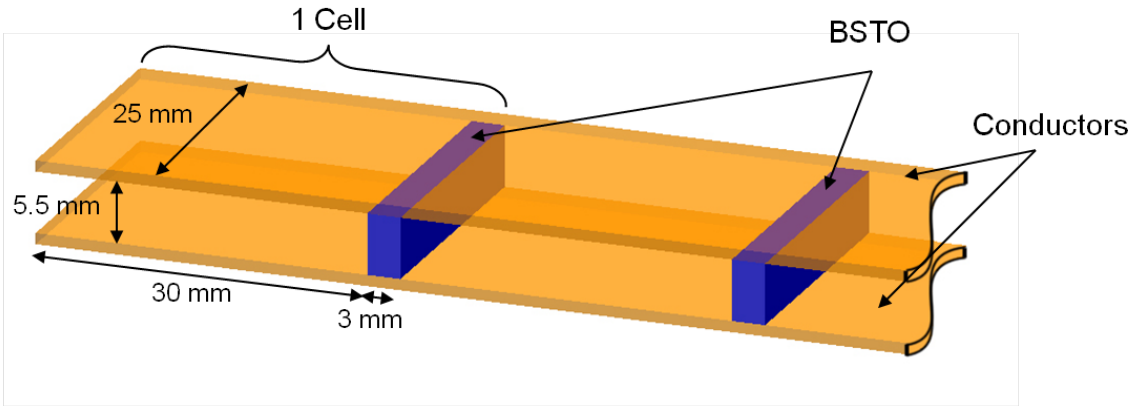

Figure 32: Schematic of Ikezi 200 - 400 MHz NLTL line[11]. This line had 24 cells/stages and was 80 cm long.

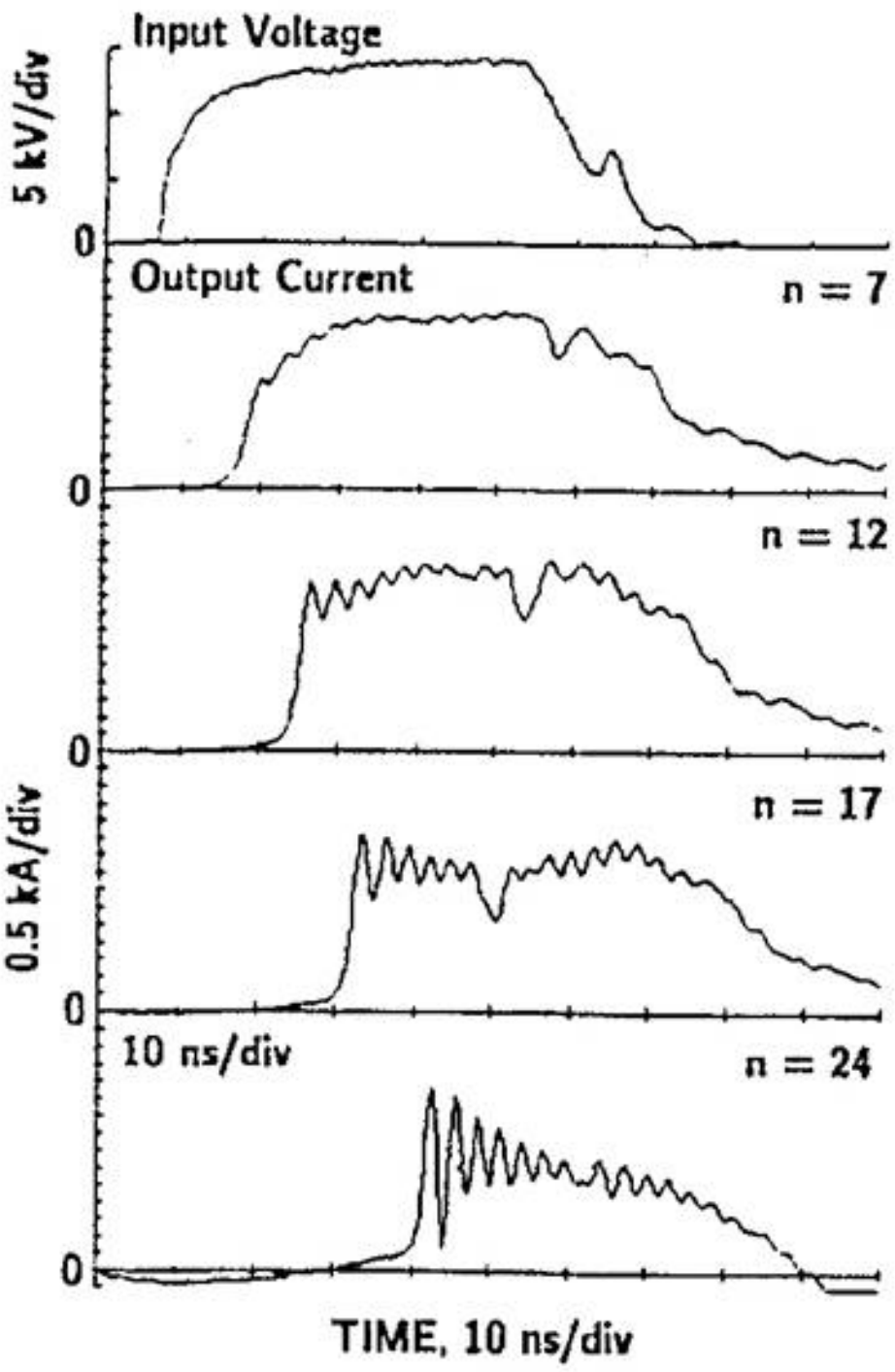

Figure 33: Measured output from the Ikezi line in Figure 30 [11].

NLTL Power Output: Resistive versus Reactive Output Loads

NLTL are inherently non-linear devices. It's why they work. However, this presents a problem because they present a non-linear impedance. Typically, we want to extract the microwaves generated by an NLTL and extract them to a linear devices, such as a linear transmission line or an antenna. The question is, can you match an NLTL into a linear load? The answer is yes.

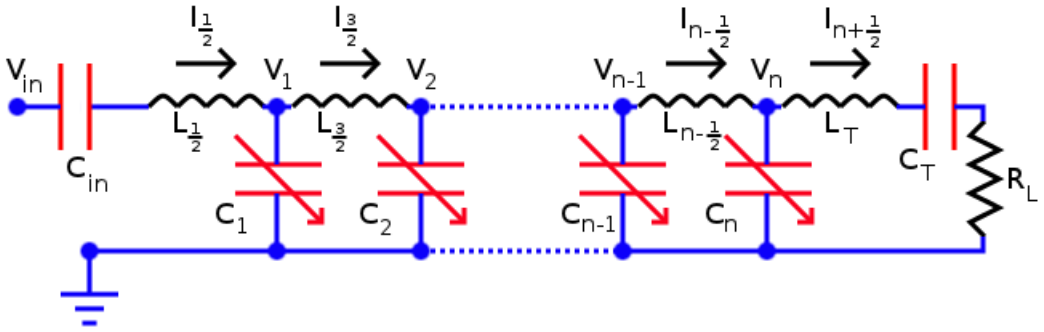

Figure 34: Terminated NLTL circuit [9].

Consider the terminated NLTL circuit shown in Figure 34. In general we terminate the NLTL with an LCR circuit where $L = L_t$, $C = C_t$ and $R = R_L$. For now let us assume that $C_t = 0$ so that we have a purely resistive, linear load. It has been shown that if we set $L_T = \frac{L}{2}$, where L is the value of the interior inductors, then almost 100% of the NLTL power can be coupled into R_L [13]. However, this type of load does effect the efficiency of the NLTL. In Figure 35 we show a simulation of an NLTL terminated by a purely resistive load. We observe that the solitons develop very nicely, until stage 90 out of 100 as the signal gets close to the load. The result is that, although the power in the NLTL is well match to the load, the conversion efficiency from the

input pulse to the RF signal is degraded. In Figure 36 we show the signal inside the resistive load, which shows both an RF signal and a substantial DC component. In Figure 37 we plot the total efficiency and RF efficiency of the line. As we can see, the maximum amount of power that is converted to RF power is 21%. This is lower than the theoretical upper limit of 33% for a uni-polar input pulse [10].

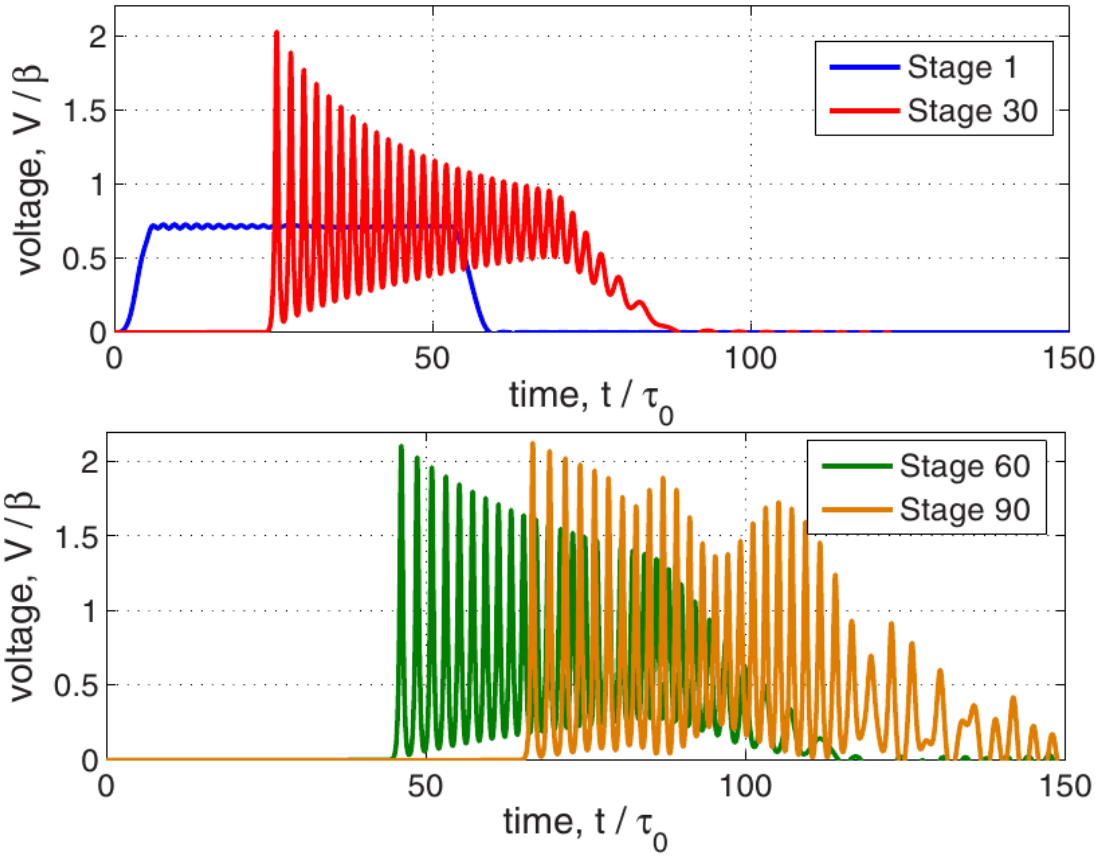

Figure 35: Evolution of a trapezoidal, uni-polar input pulse on a 100 stage NLTL terminated by a purely resistive load [9].

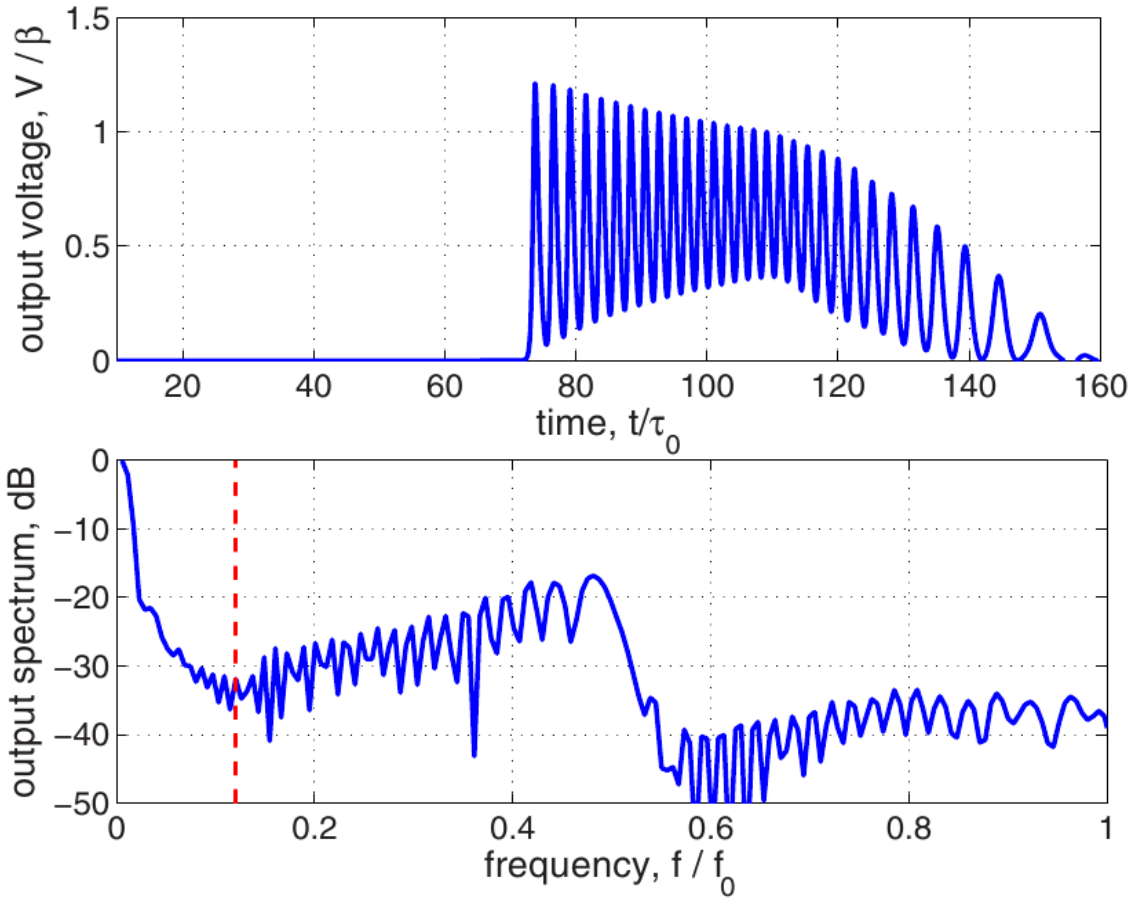

Figure 36: Signal inside the load resistor for a 100 stage NLTL terminated by a purely resistive load [9]. Note that the signal has a significant DC component.

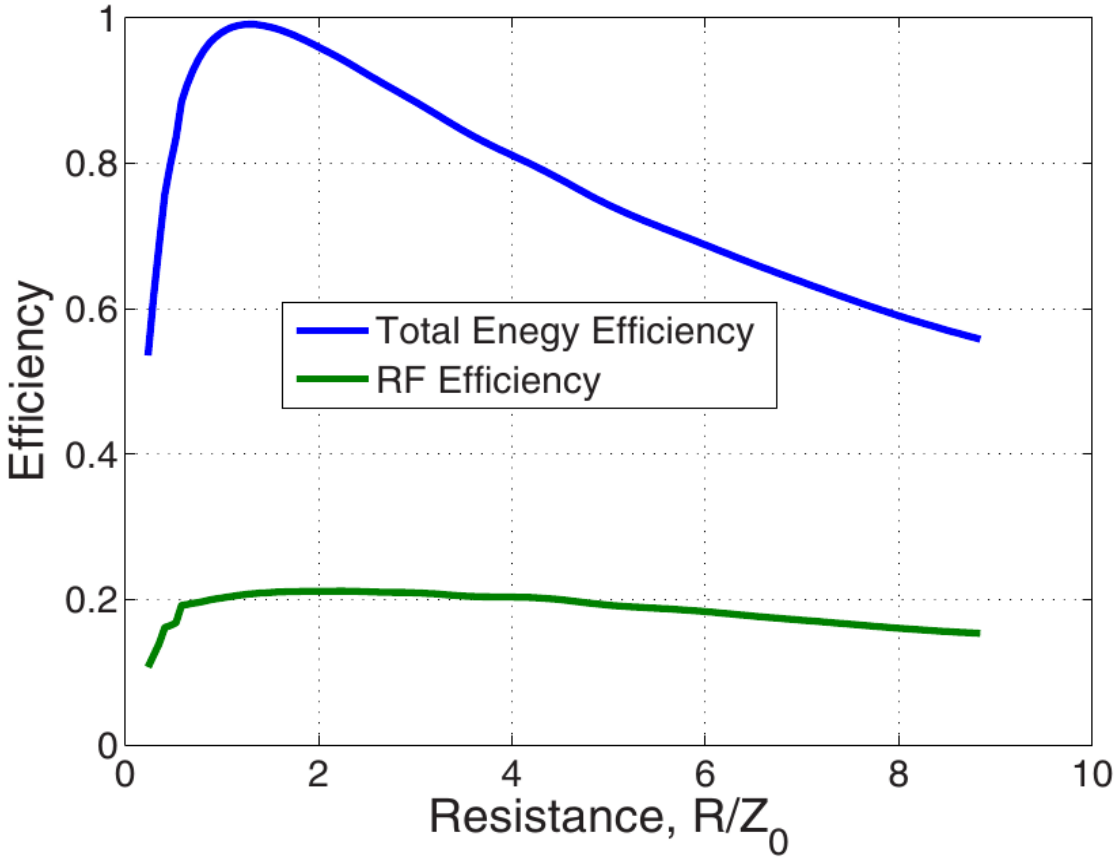

Figure 37: Efficiency of an NLTL terminated by a purely resistive, linear load [9].

A better way to terminate an NLTL is to use a reactive load by making C_T in Figure 34 non-zero. If this LCR circuit is tuned to resonant with the frequency of the NLTL, then the signal on the line looks like that shown in Figure 38. Now we see even more distortion due to the fact that the terminating LCR circuit rejects the DC component of the signal and reflects it back into the line. However [9]

- The output frequency of the NLTL is higher when terminated with hand LCR circuit as opposed to the purely resistive load.
- The RF efficiency with an LCR load is as high 30%, much higher than the peak RF efficiency for a purely resistive load.

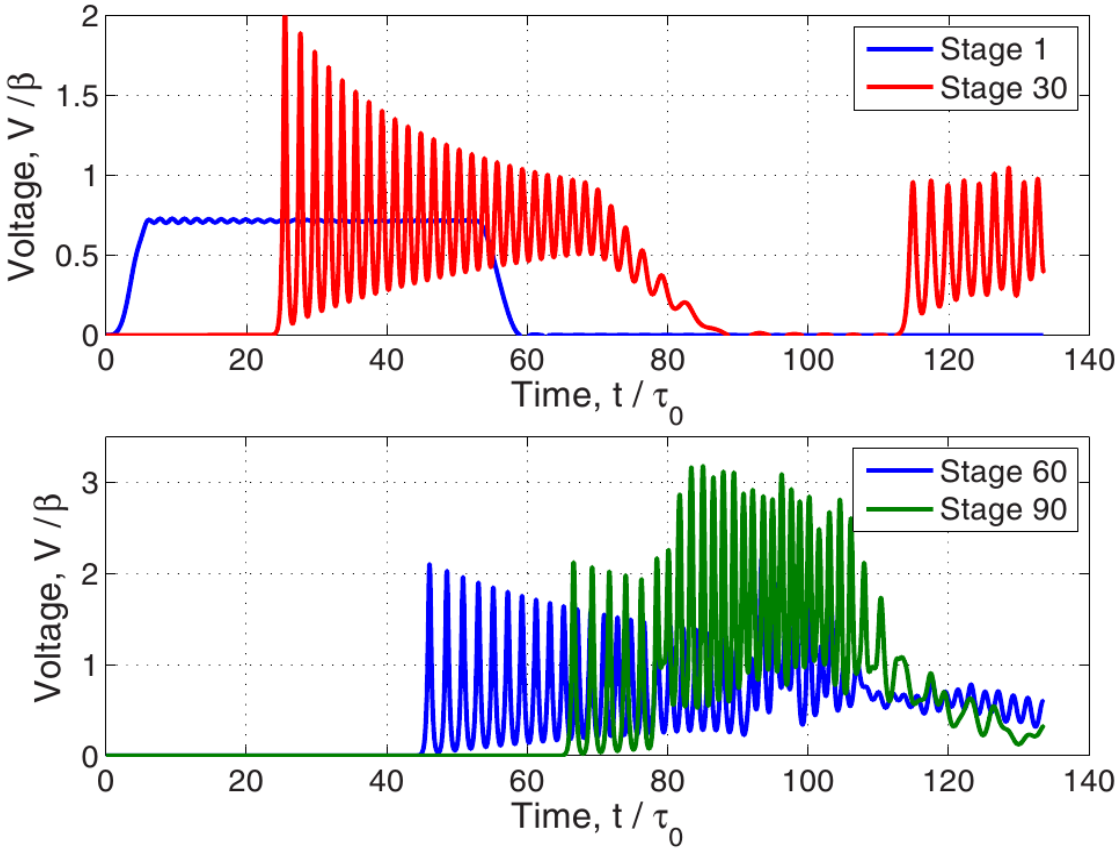

Figure 38: Evolution of a trapezoidal, uni-polar input pulse on a 100 stage NLTL terminated by a reactive, LCR circuit tuned to the line frequency [9].

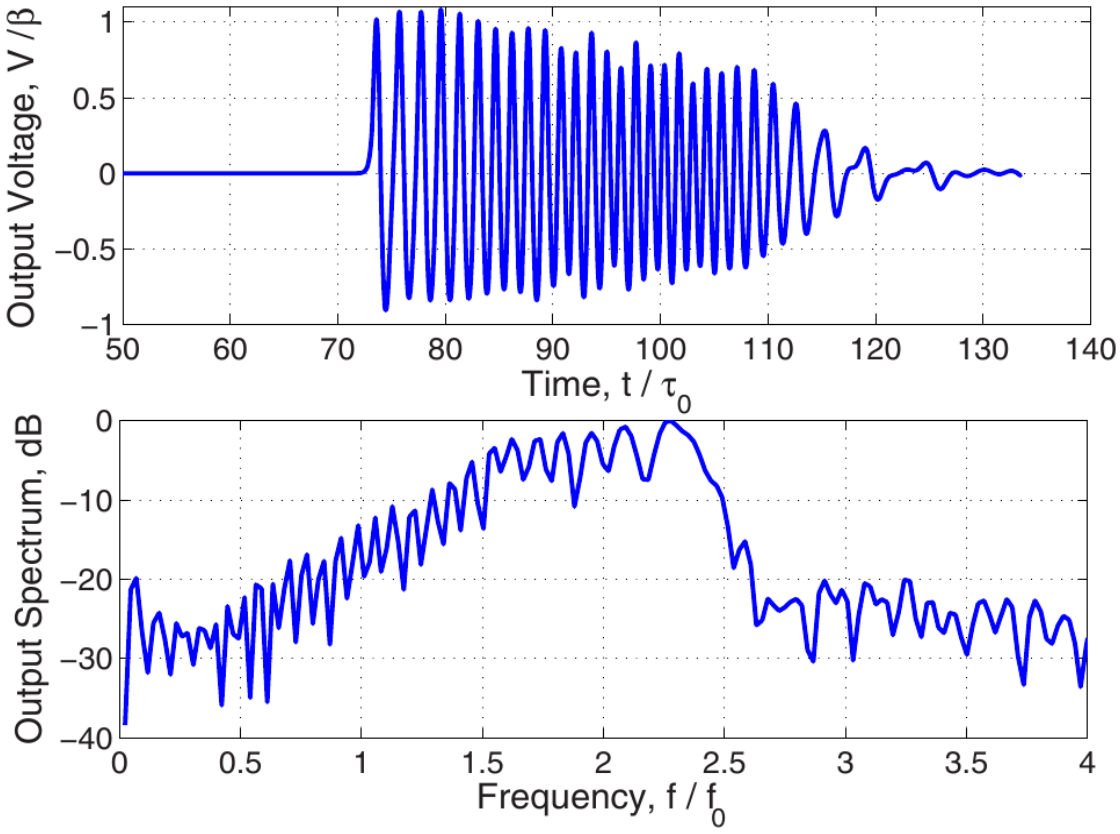

Figure 39: Signal inside the load resistor for a 100 stage NLTL terminated by a reactive, LCR circuit tune to the line frequency [9]. Note that the signal has no DC component as this part of the signal is rejected and reflected back into the NLTL.

Non-Linear Dielectrics

The heart of a high power, microwave NLTL is the non-linear dielectric. These materials dominate the performance of an NLTL. The variation of dielectric constant with applied electric field must be highly non-linear, while at the same time the electrical losses must be low enough that the RF signal is not severely impacted. It turns out these two properties are hard to find in combination.

So far, the only type of material that has been used in a microwave NLTL is called BSTO, and BSTO doped with a small amount of zirconium, BSTZO. These are ferroelectric materials whose chemical formulas are $Ba_xSr_{1-x}TiO_3$ (BSTO) and $Ba_xSr_{1-x}Ti_yZr_{1-y}O_3$ (BSTZO). The value of x is the fractional amount of Barium compared to Strontium in the BSTO or BSTZO and can vary from 0 to 1. The value of y is the fractional amount of Titanium compared to Zirconium in BSTZO and is typically equal to about 0.95. The two materials behave essentially the same for our purposes, but by adding a small amount of Zirconium to BSTO we lower the electrical losses slightly. However, pure BSTO is by far more well studied, so from this point forward we will only discuss its properties. One can assume that what follows also largely applies to BSTZO. Much of this material can be found in a review article by Tagantsev [14], which provides a good overview of ferroelectric materials in microwave applications.

Before we move on, we must first make a clarification/definition. Materials scientist distinguished between the DC relative dielectric constant, ϵ_r, which is the relative dielectric constant that we all know and love from Maxwell's equations, and the AC dielectric constant, which is more properly called the differential dielectric constant, ϵ'_r. The differential dielectric constant is defined as

$$(\epsilon'_r)_{\hat{n}} = \frac{1}{\epsilon_0}\frac{\partial P_{\hat{n}}}{\partial E_{\hat{n}}}$$

where P is the polarization of the material

$$\vec{D} = \vec{E} + \vec{P}$$

E is the electric field and $\hat{n} = \hat{x}, \hat{y}$ or $\hat{z}$. (Our material is isotropic, so keeping the vector notation is not really necessary.) The differential dielectric constant is related to the dielectric constant by

$$(\epsilon_r)_{\hat{n}} = 1 + \frac{1}{E_{\hat{n}}} \int^{E_{\hat{n}}} (\epsilon'_r)_{\hat{n}}$$

As it turns out, it is much easier to measure ϵ'_r and so materials scientist pretty much use ϵ'_r exclusively and just call it the dielectric constant. So, for the rest of this discussion, we will talk about ϵ'_r.

In Figure 40 we show a plot of ϵ'_r versus temperature for BSTO for various values of x [15]. As we see, the dielectric constant is very sensitive to temperature and can become quite high. At the peak of ϵ'_r, called the Curie point, BSTO changes phase from a ferroelectric to a paraelectric material. (The paraelectric phase is to the right of the peak.) For an NLTL, we want the BSTO to be in it's paraelectric phase.

In the paraelectric phase, ϵ'_r of BSTO demonstrates a highly non-linear response to the applied electric field. This is demonstrated in Figure 41. As we move away from the Curie temperature, this response curve flattens. So, an NLTL is typically operated slightly above the Curie temperature. This is a good property of BSTO.

Unfortunately, the properties that make BSTO (and other ferroelectric materials) good non-linear dielectrics also tend to make them more lossy than typical dielectrics used in microwave applications. In Figure 42 we show the loss tangent, $\tan(\delta)$, for BSTO. A typical microwave dielectric will have $\tan(\delta) < 0.001$, and we can see from Fig-

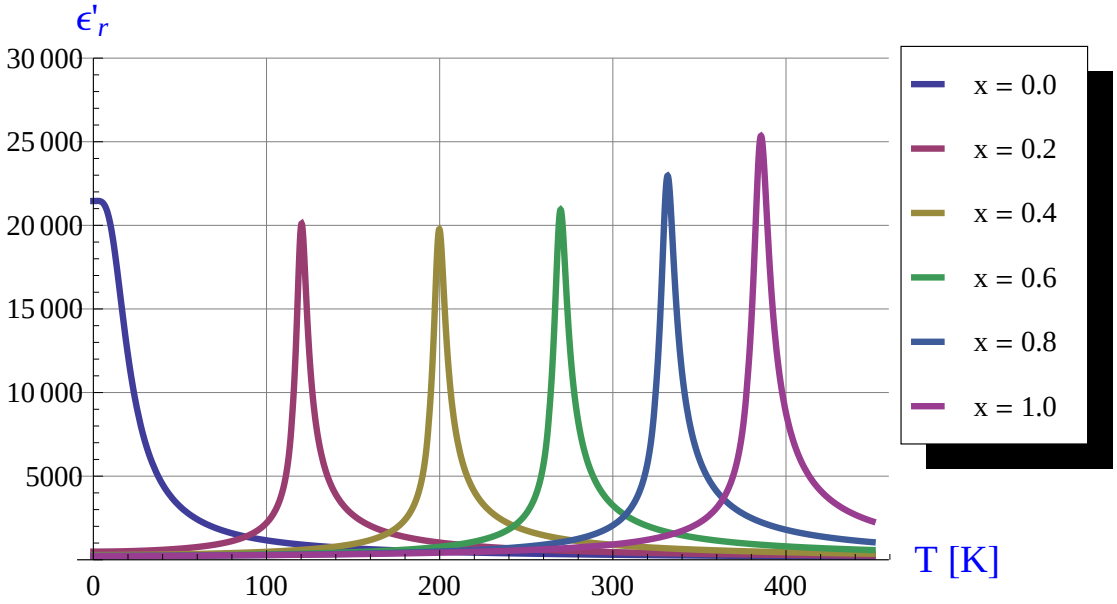

Figure 40: Differential dielectric constant of BSTO as a function of temperature for various values of the proportionality constant, x [15].

ure 42 that $\tan(\delta) > 0.001$ for BSTO. In Figures 43 and 44 we show how the high values of $\tan(\delta)$ effect NLTL performance. What we have learned is that, although BSTO has good non-linear properties, it's loss properties really are not as good as we would like. Our efficiency for BSTO based NLTs is limited to below 40%, even for a bi-polar input. The conclusion is that the non-linear dielectric part of NLTLs is still a component in need of improvement.

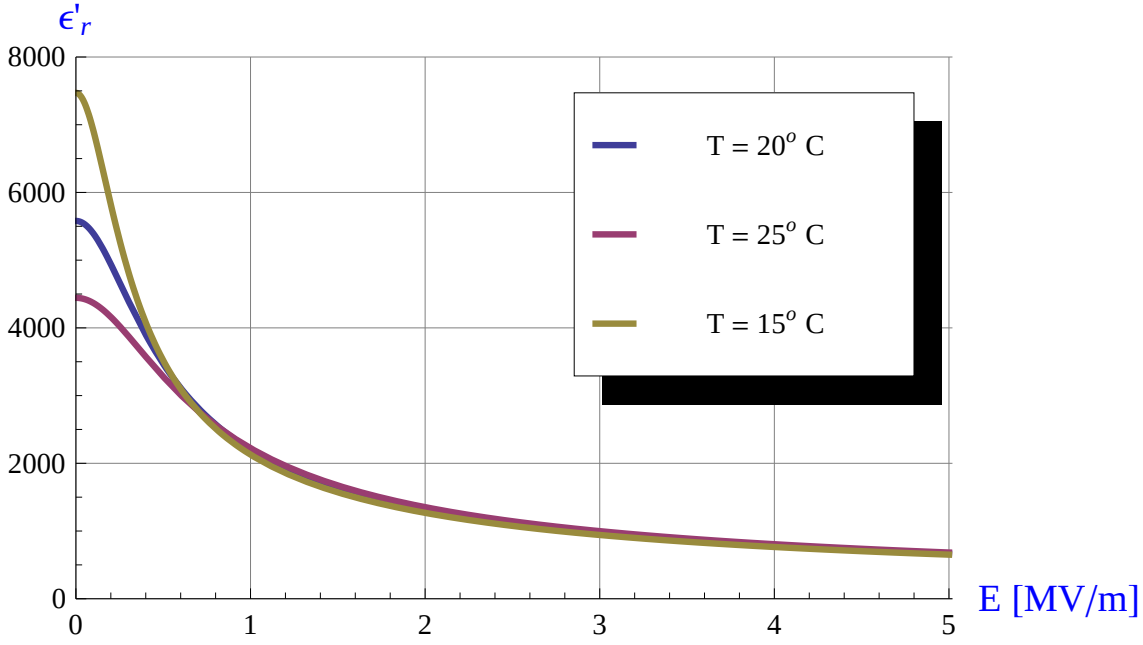

Figure 41: Differential dielectric constant of BSTO when $x = 0.62$ for three temperatures just greater than the Curie temperature as a function of the applied electric field [15].

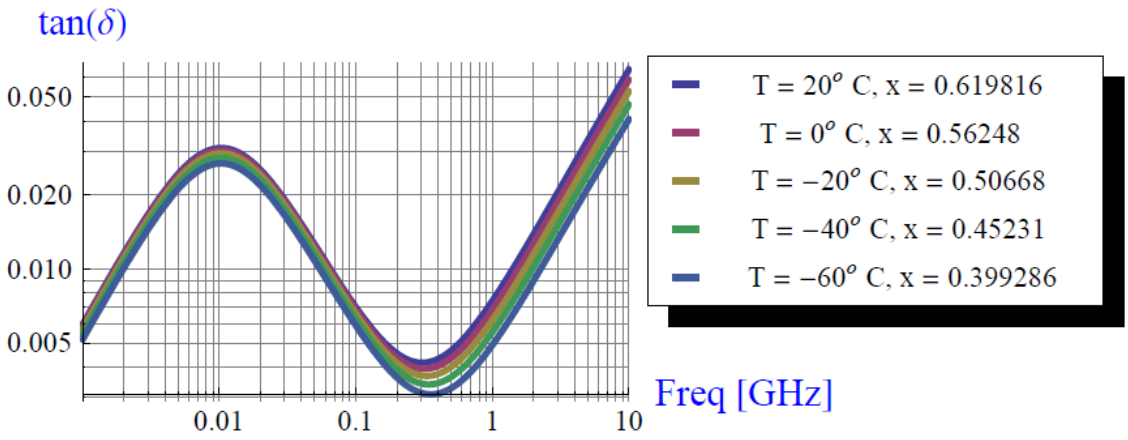

Figure 42: Dielectric loss parameter $\tan(\delta)$ (ratio of the imaginary and real components of the differential dielectric constant) for various formulations of BSTO at several temperatures versus frequency[15].

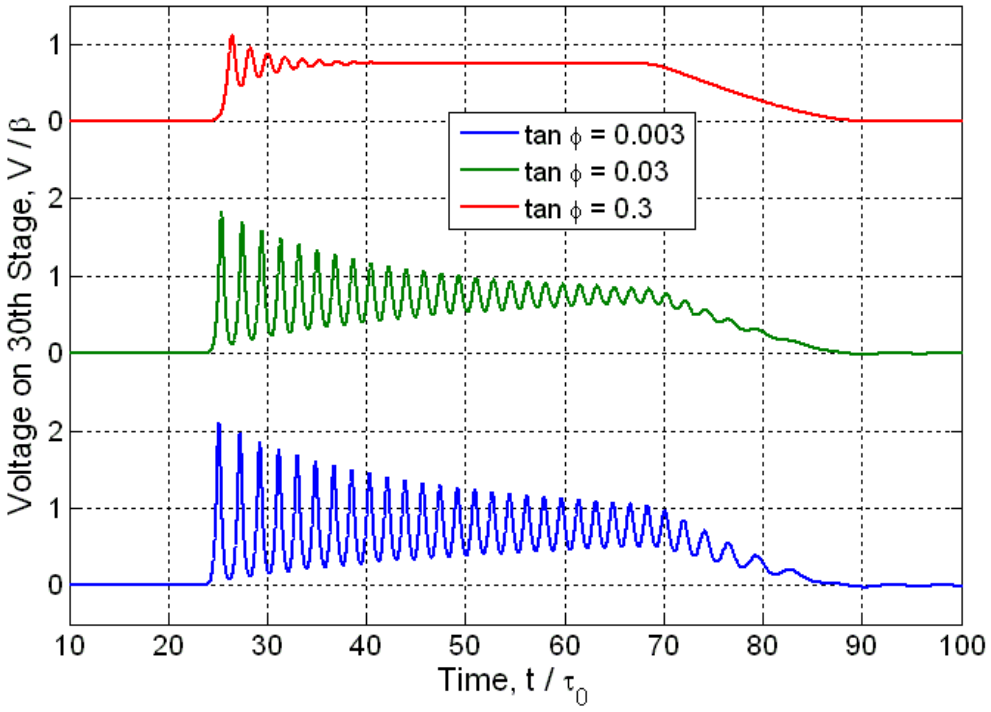

Figure 43: Simulations of the effect of tan(δ) on NLTL performance.

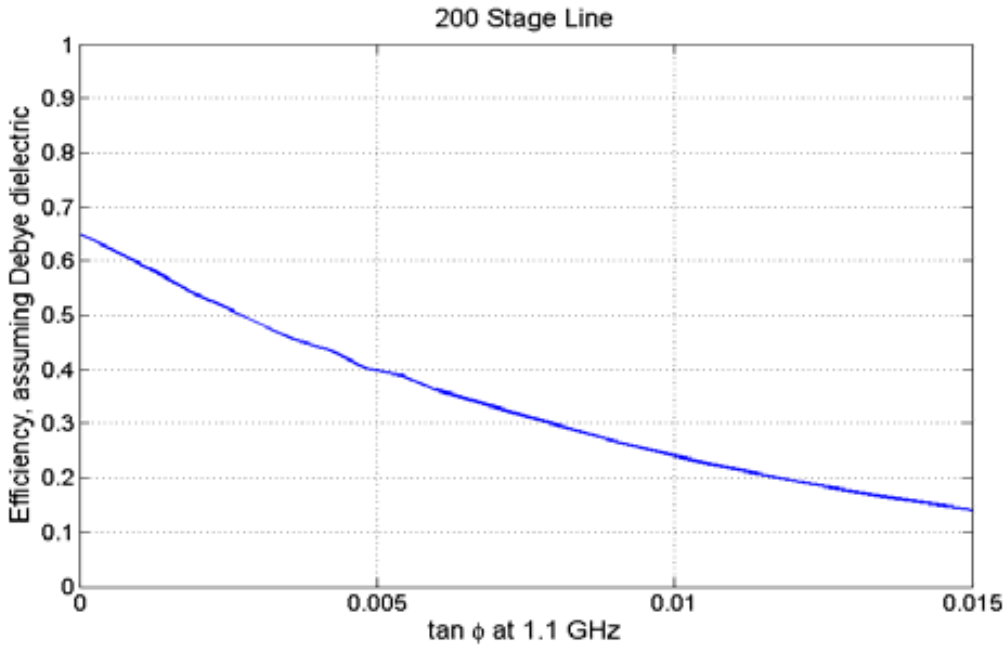

Figure 44: Effect of tan(δ) on NLTL efficiency.

Bibliography

[1] J. S. Russell, *Report on Waves*, Report of the 14^{th} Meeting of the British Association for the Advancement of Science, p. 311 (1844).

[2] D. J. Korteweg and G. de Vries, *On the Change of Form of Long Waves Advancing in a Rectangular Canal and on a New Type of Long Stationary Wave*, Philosophical Magazine, 5th series **39**, p. 422 (1895).

[3] http://www.ussdiscovery.com/FalacoSolitonMagnetic001.htm

[4] C. Weiss, *Resonator-Solitons carry information*, PTB news, **04.1** (2004).

[5] M. Brown, *High voltage soliton production in nonlinear transmissioin lines and other pulsed power applications*, Doctor of Philosophy Theses, Oriel College, September 1997.

[6] H. Washimi and T. Taniuti, *Propagation of ion-acoustic solitary waves of small amplitude*, Physical Review Letters, **17**(19), p. 996 (1966).

[7] P.G. Drazin, editor, *Solitons*, (Academic, New York) 1978.

[8] H. Nagashima and Y. Amagishi, *Experiment on the Toda Lattice Using Nonlinear Transmission Lines*, Journal of the Physical Society of Japan, **45**, No. 2, p. 680 (1978).

[9] Q. R. Marksteiner, B. Carlsten and S. Russell, *Numerical calculations of RF efficiency from a soliton generating nonlinear transmission line*, Journal of Applied Physics, **106**, Issue 11, p. 113306 (2009)

[10] Q. Marksteiner, B. Carlsten and S. Russell, *Efficient generation of RF using a biased soliton generating nonlinear transmission line with a bipolar input*, Microwave and Optical Technology Letters, **52**, Issue 6, p. 1411 (2010).

[11] H. Ikezi, J. S. DeGrassie and J. Drake, *Soliton generation at 10 MW level in the very high frequency band*, Applied Physics Letters, **58**, Issue 9, p. 986 (1991).

[12] M. P. Brown and P. W. Smith, Proceedings of the 11^{th} IEEE International Pulsed Power Conference, **1**, p. 346 (1997).

[13] Y. R. Lin-Liu, V. S. Chan, J. S. deGrassie and H. Ikezi, Microwave and Optical Technology Letters, **4**, p. 468 (1991).

[14] A.K. Tagantsev, V.O. Sherman, K.F. Astafiev, J. Venkatesh and N. Setter, *Ferroelectric Materials for Microwave Tunable Applications*, J. Electroceram., **11**, p. 5 (2003).

[15] O.G. Vendik, S.P. Zubko and M.A. Nikol'ski, *Microwave loss-factor of $Ba_xSr_{1-x}TiO_3$ as a function of temperature, biasing field, barium concentration, and frequency*, J. Appl. Phys., **92**, p. 7448 (2002).